The Journal of Chemical Physics ARTICLE scitation.org/journal/jcp

Symmetry-based singlet–triplet excitation in solution nuclear magnetic resonance

Cite as: J. Chem. Phys. **157**, 000000 (2022); doi: 10.1063/5.0103122
Submitted: 14 June 2022 • Accepted: 24 August 2022 •
Published Online: 9 99 9999

View Online Export Citation CrossMark

Mohamed Sabba,[1] Nino Wili,[2] Christian Bengs,[1] James W. Whipham,[1] Lynda J. Brown,[1] and Malcolm H. Levitt[1,a)]

AFFILIATIONS

[1] School of Chemistry, University of Southampton, Southampton SO17 1BJ, United Kingdom
[2] Interdisciplinary Nanoscience Center (iNANO) and Department of Chemistry, Aarhus University, Gustav Wieds Vej 14, DK-8000 Aarhus C, Denmark

[a)] **Author to whom correspondence should be addressed:** mhl@soton.ac.uk

ABSTRACT

Coupled pairs of spin-1/2 nuclei support one singlet state and three triplet states. In many circumstances, the nuclear singlet order, defined as the difference between the singlet population and the mean of the triplet populations, is a long-lived state that persists for a relatively long time in solution. Various methods have been proposed for generating singlet order, starting from nuclear magnetization. This requires the stimulation of singlet-to-triplet transitions by modulated radiofrequency fields. We show that a recently described pulse sequence, known as PulsePol [Schwartz *et al.*, Sci. Adv., **4**, eaat8978 (2018)], is an efficient technique for converting magnetization into long-lived singlet order. We show that the operation of this pulse sequence may be understood by adapting the theory of symmetry-based recoupling sequences in magic-angle-spinning solid-state nuclear magnetic resonance (NMR). The concept of riffling allows PulsePol to be interpreted by using the theory of symmetry-based pulse sequences and explains its robustness. This theory is used to derive a range of new pulse sequences for performing singlet–triplet excitation and conversion in solution NMR. Schemes for further enhancing the robustness of the transformations are demonstrated.

I. INTRODUCTION

Long-lived states are configurations of nuclear spin state populations, which, under suitable circumstances, are protected against important dissipation mechanisms and, therefore, persist for unusually long times in solution.[1–42] The seminal example is the *singlet order* of spin-1/2 pair systems, which is defined as the population imbalance between the spin $I = 0$ nuclear singlet state of the spin pair and the spin $I = 1$ triplet manifold.[7,13] Nuclear singlet order may be exceptionally long-lived, with decay time constants exceeding 1 h in special cases.[16] The phenomenon of long-lived nuclear spin order has been used for a variety of purposes in solution nuclear magnetic resonance (NMR), including the study of slow processes such as chemical exchange,[4,26] molecular transport,[27–30] and infrequent ligand binding to biomolecules,[31–34] as well as quantum information processing.[41,42] The dynamics of nuclear singlet states is also central to the exploitation of parahydrogen spin order in hyperpolarized NMR experiments.[36–38,43–47] Singlet NMR has also been applied to imaging and *in vivo* experiments,[23,25,35,48–55] and related techniques such as spectral editing[56,57] and low-field spectroscopy.[12,58–60]

Several methods exist for converting nuclear magnetization into singlet order in the "weak coupling" regime, meaning that the difference in the chemically shifted Larmor frequencies greatly exceeds the J-coupling between the members of the spin pair.[2–4] Methods for the "near-equivalent" and "intermediate coupling" regimes (where the chemical shift frequency difference is weaker or comparable to the J-coupling) include the magnetization-to-singlet (M2S) pulse sequence[5,6] and variants such as gM2S[24] and gc-M2S,[23] the spin-lock-induced crossing (SLIC) method,[9–12] and slow passage through level anticrossings.[17,18]

Recently, a new candidate sequence has emerged, namely, the *PulsePol* sequence, which was originally developed to implement electron-to-nuclear polarization transfer in the context of diamond nitrogen-vacancy magnetometry.[61–63] PulsePol is an attractively

simple repeating sequence of six resonant pulses and four interpulse delays. The Ph.D. thesis of Tratzmiller[62] reports numerical simulations in which PulsePol is used for magnetization-to-singlet conversion in the near-equivalent regime of high-field solution NMR. These simulations indicate that PulsePol could display significant advantages in robustness over some existing methods such as M2S and its variants. In this article, we report the following: (i) the confirmation of Tratzmiller's proposal by experimental tests; (ii) the use of symmetry-based recoupling theory, as used in magic-angle-spinning solid-state NMR,[64–67] for elucidating the operation of this pulse sequence and predicting new ones; (iii) the PulsePol sequence and its variants may be used to excite singlet–triplet coherences; (iv) the robustness of the singlet–triplet transformation may be enhanced further by using composite pulses.

The PulsePol sequence was originally derived using average Hamiltonian theory with an explicit solution of analytical equations.[61] In this article, we demonstrate an alternative theoretical treatment of PulsePol derived from the principles of symmetry-based recoupling in magic-angle-spinning solid-state NMR.[64–67] This theoretical relationship is surprising since the singlet-to-triplet conversion in solution NMR appears to be remote from recoupling in rotating solids. Nevertheless, as shown below, the problem of singlet–triplet conversion may be analyzed in a time-dependent interaction frame in which the nuclear spin operators acquire a periodic time dependence through the action of the scalar spin–spin coupling. The time-dependent spin operators in the interaction frame may be treated in a similar fashion to the anisotropic spin interactions in rotating solids, in which case the periodic time dependence is induced by the mechanical rotation of the sample. In both contexts, selection rules for the average Hamiltonian terms may be engineered by imposing symmetry constraints on the applied pulse sequences.

One common implementation of PulsePol corresponds to the pulse sequence symmetry designated as $R4_3^1$ by using the notation developed for symmetry-based recoupling.[64–67] As shown below, the spin dynamical selection rules associated with $R4_3^1$ symmetry explain the main properties of the PulsePol sequence. Furthermore, this description immediately predicts the existence of many other sequences with similar properties. Some of these novel sequences are demonstrated below.

PulsePol deviates from the standard construction procedure for symmetry-based recoupling sequences in solids. The deviation is subtle but invests PulsePol with improved robustness. Incorporating composite pulses can increase the robustness further.

II. THEORY

A. Spin Hamiltonian

The rotating-frame spin Hamiltonian for a homonuclear two-spin-1/2 system in high-field solution NMR may be written as

$$H(t) = H_{CS} + H_J + H_{rf}(t), \tag{1}$$

where the chemical shift Hamiltonian is given by

$$H_{CS} = H_\Sigma + H_\Delta \tag{2}$$

and the individual Hamiltonian terms are

$$\begin{aligned} H_\Sigma &= \frac{1}{2}\omega_\Sigma(I_{1z} + I_{2z}), \\ H_\Delta &= \frac{1}{2}\omega_\Delta(I_{1z} - I_{2z}), \\ H_J &= \omega_J \boldsymbol{I}_1 \cdot \boldsymbol{I}_2. \end{aligned} \tag{3}$$

Here, ω_Σ is the sum of the chemically shifted resonance offsets for the two spins, ω_Δ is their difference, and $\omega_J = 2\pi J$ is the scalar spin–spin coupling (J-coupling).

The interaction of the spin pair with resonant radiofrequency fields is represented by the Hamiltonian term $H_{rf}(t)$. The rotating-frame Hamiltonian for the interaction of the nuclei with a resonant time-dependent field is given by

$$H_{rf}(t) = \omega_{nut}(t)\{\cos\phi(t)(I_{1x} + I_{2x}) + \sin\phi(t)(I_{1y} + I_{2y})\}, \tag{4}$$

where the nutation frequency ω_{nut} is proportional to the radiofrequency field amplitude.

The terms H_Σ, H_J, and H_{rf} all mutually commute. The term H_Δ, on the other hand, commutes, in general, with neither H_J nor H_{rf}. We consider here the case of "near-equivalent" spin pairs,[5,6,9] for which $|\omega_\Delta| \ll |\omega_J|$. In this case, the term H_Δ may be treated as a perturbation of the dominant terms H_J and H_{rf}.

B. Propagators

The propagator $U_\Lambda(t)$ generated by a Hamiltonian term H_Λ is a unitary time-dependent operator solving the differential equation

$$\frac{\mathrm{d}}{\mathrm{d}t}U_\Lambda(t) = -iH_\Lambda(t)U_\Lambda(t) \tag{5}$$

with the boundary condition $U_\Lambda(0) = 1$. Since H_{rf} and H_J commute, the propagator $U(t)$ under the total Hamiltonian of Eq. (1) may be written as follows:

$$U(t) = U_J(t)U_{rf}(t)\widetilde{U}_{CS}(t), \tag{6}$$

where the propagator $\widetilde{U}_{CS}(t)$ solves the differential equation

$$\frac{\mathrm{d}}{\mathrm{d}t}\widetilde{U}_{CS}(t) = -i\widetilde{H}_{CS}(t)\widetilde{U}_{CS}(t) \tag{7}$$

with the boundary condition $\widetilde{U}_{CS}(0) = 1$. The interaction-frame chemical shift Hamiltonian $\widetilde{H}_{CS}(t)$ is defined as follows:

$$\widetilde{H}_{CS}(t) = U_{rf}(t)^\dagger U_J(t)^\dagger H_{CS} U_J(t) U_{rf}(t). \tag{8}$$

Equation (8) shows that the chemical shift terms acquire a double modulation in the interaction frame: first from the action of the J-coupling, and second from the action of the applied rf field.

Since the J-coupling is time-independent, the propagator U_J has the following form:

$$U_J(t) = \exp\{-iH_J t\} = \exp\{-i\omega_J t \boldsymbol{I}_1 \cdot \boldsymbol{I}_2\}. \tag{9}$$

The singlet and triplet states of the spin-1/2 pair are defined as follows:

$$\begin{aligned} |S_0\rangle &= 2^{-1/2}(|\alpha\beta\rangle - |\beta\alpha\rangle), \\ |T_{+1}\rangle &= |\alpha\alpha\rangle, \\ |T_0\rangle &= 2^{-1/2}(|\alpha\beta\rangle + |\beta\alpha\rangle), \\ |T_{-1}\rangle &= |\beta\beta\rangle. \end{aligned} \tag{10}$$

Since the singlet and triplet states are eigenstates of H_J, with eigenvalues $-3\omega_J/4$ and $+\omega_J/4$, respectively, the propagator U_J may be written as follows:

$$U_J(t) = \exp\left\{+i\frac{3}{4}\omega_J t\right\}|S_0\rangle\langle S_0| + \exp\left\{-i\frac{1}{4}\omega_J t\right\}\sum_M |T_M\rangle\langle T_M|. \tag{11}$$

The rf propagator $U_{\rm rf}(t)$ corresponds to a time-dependent rotation in three-dimensional space, described by three Euler angles,

$$\begin{aligned} U_{\rm rf}(t) &= R(\Omega_{\rm rf}(t)) \\ &= R_z(\alpha_{\rm rf}(t))R_y(\beta_{\rm rf}(t))R_z(\gamma_{\rm rf}(t)), \end{aligned} \tag{12}$$

with

$$R_\chi(\theta) = \exp\{-i\theta I_\chi\}. \tag{13}$$

The action of the modulated radiofrequency field on the spin system may, therefore, be described in terms of a time-dependent set of three Euler angles, $\Omega_{\rm rf}(t) = \{\alpha_{\rm rf}(t), \beta_{\rm rf}(t), \gamma_{\rm rf}(t)\}$.

In general, it is possible to modulate the amplitude $\omega_{\rm nut}(t)$ and the phase $\phi(t)$ of the rf field in time, in order to generate any desired trajectory of Euler angles $\Omega_{\rm rf}(t)$.

C. Spherical tensor operators

It is convenient to define two spherical tensor spin operators of rank-1, denoted as $\mathbb{T}^g_1$ and $\mathbb{T}^u_1$, where the superscripts denote their parity under exchange of the two spin-1/2 particles as follows:

$$\begin{aligned} (12)\mathbb{T}^g_{1m}(12)^\dagger &= \mathbb{T}^g_{1m}, \\ (12)\mathbb{T}^u_{1m}(12)^\dagger &= -\mathbb{T}^u_{1m}, \end{aligned} \tag{14}$$

where $m \in \{+1, 0, -1\}$ and (12) denotes the particle exchange operator. The *gerade* spherical tensor operator is constructed from the total angular momentum and shift operators for the spin system,

$$\begin{aligned} \mathbb{T}^g_{1+1} &= -2^{-1/2}(I_1^+ + I_2^+), \\ \mathbb{T}^g_{10} &= I_{1z} + I_{2z}, \\ \mathbb{T}^g_{1-1} &= 2^{-1/2}(I_1^- + I_2^-). \end{aligned} \tag{15}$$

The *ungerade* spherical tensor operator of rank-1 plays a prominent role in the current theory. It has the following components:

$$\begin{aligned} \mathbb{T}^u_{1+1} &= |T_{+1}\rangle\langle S_0|, \\ \mathbb{T}^u_{10} &= |T_0\rangle\langle S_0|, \\ \mathbb{T}^u_{1-1} &= |T_{-1}\rangle\langle S_0|. \end{aligned} \tag{16}$$

Each component is given by a shift operator between the singlet state and one of the three triplet states. The adjoint operators are given by

$$\begin{aligned} \mathbb{T}^{u\dagger}_{1+1} &= |S_0\rangle\langle T_{+1}|, \\ \mathbb{T}^{u\dagger}_{10} &= |S_0\rangle\langle T_0|, \\ \mathbb{T}^{u\dagger}_{1-1} &= |S_0\rangle\langle T_{-1}|. \end{aligned} \tag{17}$$

Both sets of operators $\mathbb{T}^g_1$ and $\mathbb{T}^u_1$ transform irreducibly under the three-dimensional rotation group,

$$\begin{aligned} R(\Omega)\mathbb{T}^g_{1\mu}R^\dagger(\Omega) &= \sum_{\mu'=-1}^{+1}\mathbb{T}^g_{1\mu'}\mathscr{D}^1_{\mu'\mu}(\Omega), \\ R(\Omega)\mathbb{T}^u_{1\mu}R^\dagger(\Omega) &= \sum_{\mu'=-1}^{+1}\mathbb{T}^u_{1\mu'}\mathscr{D}^1_{\mu'\mu}(\Omega). \end{aligned} \tag{18}$$

Here, $\mathscr{D}^\lambda_{\mu'\mu}(\Omega)$ represents an element of the rank-λ Wigner rotation matrix.[68]

The *gerade* spherical tensor operator $\mathbb{T}^g_1$ obeys the standard relationship between its components under the adjoint transformation,[68]

$$\mathbb{T}^{g\dagger}_{1\mu} = (-1)^\mu\mathbb{T}^g_{1-\mu}. \tag{19}$$

However, the analogous relationship does *not* apply to the components of the *ungerade* spherical tensor operator $\mathbb{T}^u_1$.

D. Interaction frame Hamiltonian

The chemical shift Hamiltonian terms, given in Eq. (3), may be written in terms of the $m = 0$ spherical tensor operator components as follows:

$$\begin{aligned} H_\Sigma &= \frac{1}{2}\omega_\Sigma\mathbb{T}^g_{10}, \\ H_\Delta &= \frac{1}{2}\omega_\Delta\left(\mathbb{T}^u_{10} + \mathbb{T}^{u\dagger}_{10}\right). \end{aligned} \tag{20}$$

From Eq. (11), these operators transform as follows under the propagator U_J:

$$\begin{aligned} U_J^\dagger(t)H_\Sigma U_J(t) &= \frac{1}{2}\omega_\Sigma\mathbb{T}^g_{10}, \\ U_J^\dagger(t)H_\Delta U_J(t) &= \frac{1}{2}\omega_\Delta\left(\mathbb{T}^u_{10}\exp\{+i\omega_J t\} + \mathbb{T}^{u\dagger}_{10}\exp\{-i\omega_J t\}\right). \end{aligned} \tag{21}$$

This may be combined with Eqs. (8), (12), and (18) to obtain the following expression for the interaction-frame chemical shift Hamiltonian:

$$\widetilde{H}_{\rm CS}(t) = \sum_{m=-1}^{+1}\sum_{\mu=-1}^{+1}\widetilde{H}_{1m1\mu}(t), \tag{22}$$

where each term has the form

$$\widetilde{H}_{1m1\mu}(t) = \omega_{1m1\mu}d^1_{\mu0}(-\beta_{\rm rf}(t))\exp\{i(m\omega_J t + \mu\gamma_{\rm rf}(t))\}Q_{1m1\mu} \tag{23}$$

in which $d^1_{\mu0}(\beta)$ is an element of the rank-1 reduced Wigner matrix. The amplitudes $\omega_{1m1\mu}$ and spin operators $Q_{1m1\mu}$ take the following values:

$$\omega_{1\,+1\,1\mu} = \frac{1}{2}\omega_{\Delta}, \qquad Q_{1\,+1\,1\mu} = \mathbb{T}^{u}_{1\mu},$$
$$\omega_{1\,0\,1\mu} = \frac{1}{2}\omega_{\Sigma}, \qquad Q_{1\,0\,1\mu} = \mathbb{T}^{g}_{1\mu}, \tag{24}$$
$$\omega_{1\,-1\,1\mu} = \frac{1}{2}\omega_{\Delta}, \qquad Q_{1\,-1\,1\mu} = (-1)^{\mu}\mathbb{T}^{u\dagger}_{1\,-\mu},$$

where $\mu \in \{+1, 0, -1\}$. Note that the singlet–triplet excitation terms have quantum number $m = \pm 1$, while the resonance offset term has $m = 0$.

For the terms $\omega_{\ell m\lambda\mu}$ and $Q_{\ell m\lambda\mu}$ above, the rank of the interaction under rotations of the spins is specified as $\lambda = 1$. On the other hand, the "pseudo-space-rank" $\ell = 1$ has no physical meaning and is introduced to establish a correspondence with the notation used in magic-angle-spinning solid-state NMR.[64–67]

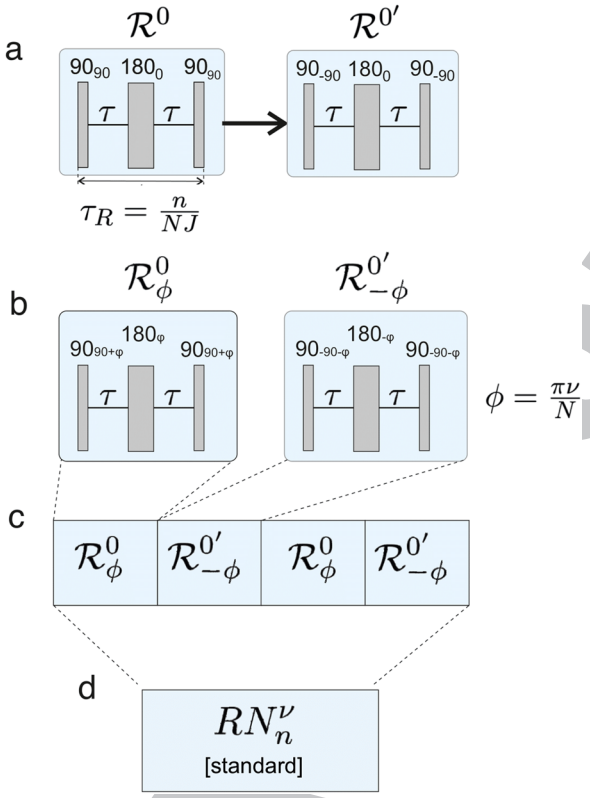

FIG. 1. Standard implementation of an RN^{ν}_{n} sequence for singlet–triplet conversion. (a) A basic *R*-element denoted $\mathscr{R}^0$ is selected. This element induces a rotation about the rotating-frame x-axis through an odd multiple of π. In the current case, the element $\mathscr{R}^0$ is given by the composite pulse $90_{90}180_{0}90_{90}$ with delays τ between the pulses such that its overall duration is $\tau_R = n/(NJ)$. The conjugate sequence $\mathscr{R}^{0'}$ is generated from $\mathscr{R}^0$ by a change in the sign of all phases. (b) The sequence $\mathscr{R}^0$ is given a phase shift of $+\phi$, while the sequence $\mathscr{R}^{0'}$ is given a phase shift of $-\phi$, where $\phi = \pi\nu/N$. (c) The pair of sequences $(\mathscr{R}^0)_{\phi}$ and $(\mathscr{R}^{0'})_{-\phi}$ is repeated $N/2$ times to give the standard implementation of an RN^{ν}_{n} sequence (d).

E. Symmetry-based sequences

Symmetry-based pulse sequences[64–67] were originally developed for magic-angle-spinning solid-state NMR, where the sample is rotated mechanically with the angular frequency ω_r such that its rotational period is given by $\tau_r = |2\pi/\omega_r|$. In the current case of singlet–triplet excitation in solution NMR, the J-coupling plays the role of the mechanical rotation. The relevant period is therefore given by $\tau_J = |2\pi/\omega_J| = |J^{-1}|$.

In the current context, a sequence with RN^{ν}_{n} symmetry is defined by the following time-symmetry relationship of the rf Euler angles $\beta_{\rm rf}(t)$ and $\gamma_{\rm rf}(t)$, which applies for arbitrary time points t,[64–67]

$$\beta_{\rm rf}\left(t + \frac{n\tau_J}{N}\right) = \beta_{\rm rf}(t) \pm \pi,$$
$$\gamma_{\rm rf}\left(t + \frac{n\tau_J}{N}\right) = \gamma_{\rm rf}(t) - \frac{2\pi\nu}{N}. \tag{25}$$

A complete RN^{ν}_{n} sequence has a duration of $T = n\tau_J$, and is cyclic, in the sense that the net rotation induced by the rf field over the complete sequence is through an even multiple of π.

The *symmetry numbers* N, n, and ν take integer values. In the case of RN^{ν}_{n} sequences, N must be even, while n and ν are unconstrained. As discussed below, the symmetry numbers define the selection rules for the spin dynamics under the pulse sequence.

The RN^{ν}_{n} Euler angle symmetries in Eq. (25) do not define the pulse sequence uniquely. Nevertheless, there is a standard procedure[64–67] for generating these Euler angle symmetries, which is sketched in Fig. 1. The procedure is as follows:

- Select an rf pulse sequence, known as a *basic R-element*, designated as $\mathscr{R}^0$. This sequence may be arbitrarily complex, but must induce a net rotation of the resonant spins by an odd multiple of π about the rotating-frame x-axis. If the duration of the basic element $\mathscr{R}^0$ is denoted as τ_R, this implies the condition

$$U_{\rm rf}(\tau_R) = R_x(p\pi), \tag{26}$$

  where p is an odd integer.
- The duration of the basic element τ_R is given by $\tau_R = (n/N)J^{-1}$, where n and N are the symmetry numbers of the RN^{ν}_{n} sequence.
- Reverse the sign of all phases in $\mathscr{R}^0$. This leads to the *conjugate element* designated $\mathscr{R}^{0'}$.
- Give all components of the basic element $\mathscr{R}^0$ a phase shift of $+\pi\nu/N$. This gives the phase-shifted basic element denoted as $\mathscr{R}^0_{+\pi\nu/N}$.
- Give all components of the conjugate element $\mathscr{R}^{0'}$ a phase shift of $-\pi\nu/N$. This gives the element $\mathscr{R}^{0'}_{-\pi\nu/N}$.
- The complete RN^{ν}_{n} sequence is composed of $N/2$ repeats of the element pair, as follows:

$$RN^{\nu}_{n} = \{\mathscr{R}^0_{+\pi\nu/N}\mathscr{R}^{0'}_{-\pi\nu/N}\}^{N/2}. \tag{27}$$

The complete RN^{ν}_{n} sequence has an overall duration of

$$T = N\tau_R = nJ^{-1}. \tag{28}$$

F. Selection rules

The propagator for a complete RN_n^ν sequence is given from Eq. (6) by

$$U(T) = U_J(T)U_{\rm rf}(T)\widetilde{U}_{\rm CS}(T). \tag{29}$$

From the definition of an RN_n^ν sequence, the complete sequence propagators $U_J(T)$ and $U_{\rm rf}(T)$ are both proportional to the unity operator and may be ignored. The operator $\widetilde{U}_{\rm CS}(T)$ corresponds to propagation under a time-independent effective Hamiltonian,

$$\widetilde{U}_{\rm CS}(T) = \exp\{-i\overline{H}_{\rm CS}T\}. \tag{30}$$

In the near-equivalence limit ($|\omega_J| \gg |\omega_\Delta|, |\omega_\Sigma|$), the effective Hamiltonian $\overline{H}_{\rm CS}$ may be approximated by the first term in a Magnus expansion,[69,71]

$$\overline{H}_{\rm CS} \simeq \overline{H}_{\rm CS}^{(1)}, \tag{31}$$

where

$$\overline{H}_{\rm CS}^{(1)} = \sum_{m=-1}^{+1}\sum_{\mu=-1}^{+1}\overline{H}_{1m1\mu}^{(1)}. \tag{32}$$

In common with many recent papers,[64–67] this article uses a numbering of the Magnus expansion terms that differs from the older literature[69–71] by one.

The individual average Hamiltonian terms are given by

$$\overline{H}_{1m1\mu}^{(1)} = T^{-1}\int_0^T \widetilde{H}_{1m1\mu}(t)\,dt, \tag{33}$$

where the interaction frame terms $\widetilde{H}_{1m1\mu}(t)$ are given in Eq. (23).

The Euler angle symmetries in Eq. (25) lead to the following selection rules for the first-order average Hamiltonian terms of RN_n^ν sequences:[64–67]

$$\overline{H}_{\ell m\lambda\mu}^{(1)}(t_0) = 0 \quad \text{if} \quad mn - \mu\nu \neq \frac{N}{2}Z_\lambda, \tag{34}$$

where Z_λ is any integer with the same parity as λ. This selection rule may be visualized by a diagrammatic procedure.[65,66]

In the current case, $\lambda = 1$ for all relevant interactions, so that Z_λ is any odd integer. The Hamiltonian components for which $mn - \mu\nu$ is an odd multiple of $N/2$ are symmetry-allowed and may contribute to the effective Hamiltonian. A symmetry-allowed term with quantum numbers $\{m,\ \mu\}$ and ranks $\ell = \lambda = 1$ is given, in general, by

$$\overline{H}_{1m1\mu}^{(1)} = \kappa_{1m1\mu}\omega_{1m1\mu}Q_{1m1\mu}, \tag{35}$$

where the amplitudes $\omega_{1m1\mu}$ and spin operators $Q_{1m1\mu}$ are given in Eq. (24).

The scaling factor $\kappa_{\ell m\lambda\mu}$ of a symmetry-allowed term is given by

$$\kappa_{\ell m\lambda\mu} = \exp\left(-i\mu\frac{\pi\nu}{N}\right)K_{m\lambda\mu}, \tag{36}$$

where $K_{m\lambda\mu}$ is defined with respect to the basic element $\mathscr{R}^0$,

$$K_{m\lambda\mu} = \tau_R^{-1}\int_0^{\tau_R} d^\lambda_{\mu 0}(-\beta^0_{\rm rf}(t))\exp\{i(\mu\gamma^0_{\rm rf}(t) + m\omega_J t)\}dt. \tag{37}$$

Here, $\beta^0_{\rm rf}$ and $\gamma^0_{\rm rf}$ represent the Euler angles describing the rotation induced by the rf field under the basic element.[64–67]

Symmetry-based pulse sequences are designed by selecting combinations of symmetry numbers N, n, and ν such that all desirable average Hamiltonian terms $\overline{H}_{\ell m\lambda\mu}^{(1)}$ are symmetry-allowed, while all undesirable terms are symmetry-forbidden. In most cases, the basic element $\mathscr{R}^0$ is selected such that the scaling factors $\kappa_{\ell m\lambda\mu}$ are maximized for the desirable symmetry-allowed terms.

G. Transition-selective singlet–triplet excitation

Table I shows some sets of symmetry numbers $\{N, n, \nu\}$ under which the average Hamiltonian terms with quantum numbers $\{\ell, m, \lambda,\ \mu\} = \{1, \pm1, 1, \pm1\}$ are symmetry-allowed, while all other terms are symmetry-forbidden and are suppressed in the average Hamiltonian. In particular, all resonance-offset terms, which have $m = 0$, are symmetry-forbidden in the first-order average Hamiltonian, for the symmetries in Table I.

For example, consider the symmetry $R4_3^1$. The term $\{\ell, m, \lambda, \mu\} = \{1, 1, 1, 1\}$ is symmetry-allowed since the expression $nm - \nu\mu$ evaluates to $3 \times 1 - 1 \times 1 = 2$, which is an odd multiple of $N/2 = 2$. On the other hand, the term $\{\ell, m, \lambda, \mu\} = \{1, 1, 1, -1\}$ is symmetry-forbidden, since $nm - \nu\mu$ evaluates to $3 \times 1 - 1 \times (-1) = 4$, which is an *even* multiple of 2. Similarly, the resonance-offset term $\{\ell, m, \lambda, \mu\}$

TABLE I. A selection of RN_n^ν symmetries that are appropriate for symmetry-based singlet–triplet conversion in solution NMR. These symmetries select $\overline{H}_{\ell m\lambda\mu}^{(1)}$ terms with quantum numbers $\{\ell, m, \lambda,\ \mu\}$ given by $\{1, \pm1, 1, \pm1\}$. Changing the sign of ν selects the terms $\{1, \pm1, 1, \mp1\}$ instead. Scaling factors κ_{1111} are given for the basic R-element in Eq. (48), in the limit of radiofrequency pulses with negligible duration.

RN_n^ν	κ_{1111}
$R4_1^{-1}$	−0.264
$R4_3^1$	−0.512
$R4_5^{-1}$	0.307
$R4_7^1$	0.038
$R4_9^{-1}$	−0.029
$R6_1^{-2}$	−0.104
$R6_5^2$	−0.291
$R6_7^{-2}$	0.360
$R6_8^{-1}$	0.253
$R6_{10}^1$	0.068
$R8_1^{-3}$	−0.137
$R8_3^{-1}$	−0.371
$R8_5^1$	−0.498
$R8_7^3$	−0.495
$R8_9^{-3}$	0.385
$R10_1^{-4}$	−0.110
$R10_2^{-3}$	−0.215
$R10_3^{-2}$	−0.309
$R10_4^{-1}$	−0.389
$R10_6^1$	−0.491
$R10_7^2$	−0.511

$= \{1, 0, 1, -1\}$ is symmetry-forbidden since $nm - \nu\mu$ evaluates to $3 \times 0 - 1 \times (-1) = 1$, which is not an integer multiple of 2.

All symmetries in Table I select Hamiltonian components with quantum numbers $\{\ell, m, \lambda, \mu\} = \{1, \pm 1, 1, \pm 1\}$ while suppressing all other terms. In this case, the first-order average Hamiltonian is given through Eq. (24) by

$$\begin{aligned}\overline{H}^{(1)}_{\mathrm{CS}} &= \kappa_{1\,+1\,1\,+1}\omega_{1\,+1\,1\,+1}Q_{1\,+1\,1\,+1} + \kappa_{1\,-1\,1\,-1}\omega_{1\,-1\,1\,-1}Q_{1\,-1\,1\,-1}\\ &= \frac{1}{2}\omega_{\Delta}\left\{\kappa_{1+11+1}\mathbb{T}^{u}_{1\,+1} + (\kappa_{1+11+1}\mathbb{T}^{u}_{1\,+1})^{\dagger}\right\}. \qquad (38)\end{aligned}$$

Therefore, the first-order average Hamiltonian generates a selective rotation of the transition between the singlet state $|S_0\rangle$ and the lower triplet state $|T_{+1}\rangle$, as shown in Fig. 2(a),

$$\overline{H}^{(1)}_{\mathrm{CS}} = \frac{1}{2}\omega^{\mathrm{ST}}_{\mathrm{nut}}\left(e^{-i\phi_{\mathrm{ST}}}|S_0\rangle\langle T_{+1}| + e^{+i\phi_{\mathrm{ST}}}|T_{+1}\rangle\langle S_0|\right). \qquad (39)$$

The singlet–triplet nutation frequency and phase depend upon the scaling factors as follows:

$$\omega^{\mathrm{ST}}_{\mathrm{nut}} = \omega_{\Delta}|\kappa_{1+11+1}| = \omega_{\Delta}|\kappa_{1-11-1}|, \qquad (40)$$

$$\phi_{\mathrm{ST}} = \arg(\kappa_{1-11-1}) = \arg(-\kappa^{*}_{1111}). \qquad (41)$$

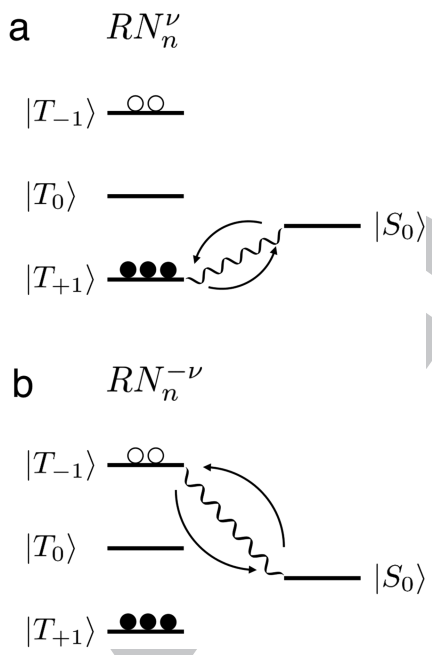

FIG. 2. Energy levels and approximate eigenstates of a *J*-coupled two-spin-1/2 system in the near-equivalence limit. (a) An RN^{ν}_{n} sequence, with symmetry numbers chosen to select terms $\{m, \mu\} = \{\pm 1, \pm 1\}$ and suppress all others, induces a transition between the $|S_0\rangle$ and $|T_{+1}\rangle$ states. Suitable symmetries are given in Table I. One example is $\mathrm{R4}^{+1}_{3}$. (b) If the symmetry number ν is changed in sign, average Hamiltonian terms with quantum numbers $\{m, \mu\} = \{\pm 1, \mp 1\}$ are selected. In this case, there is selective excitation of the transition between the $|S_0\rangle$ and $|T_{-1}\rangle$ states. One example is $\mathrm{R4}^{-1}_{3}$.

If a set of symmetry numbers $\{N, n, v\}$ selects the terms $\{\ell, m, \lambda, \mu\} = \{1, \pm 1, 1, \pm 1\}$, then the set of symmetry numbers $\{N, n, -v\}$ selects the terms $\{\ell, m, \lambda, \mu\} = \{1, \pm 1, 1, \mp 1\}$. As indicated in Fig. 2(b), the change in the sign of v leads to a selective rotation of the singlet state and the *upper* triplet state.

In either case, the dynamics of the system may be described by a two-level treatment. Define the single-transition operators[72,73] for the transitions between the singlet state and the outer triplet states as follows:

$$\begin{aligned}I^{\mathrm{ST}(\pm)}_{x} &= \frac{1}{2}(|T_{\pm1}\rangle\langle S_0| + |S_0\rangle\langle T_{\pm1}|),\\ I^{\mathrm{ST}(\pm)}_{y} &= \frac{1}{2i}(|T_{\pm1}\rangle\langle S_0| - |S_0\rangle\langle T_{\pm1}|), \qquad (42)\\ I^{\mathrm{ST}(\pm)}_{z} &= \frac{1}{2}(|T_{\pm1}\rangle\langle T_{\pm1}| - |S_0\rangle\langle S_0|).\end{aligned}$$

These operators have cyclic commutation relationships,[72,73]

$$\left[I^{\mathrm{ST}(\pm)}_{x}, I^{\mathrm{ST}(\pm)}_{y}\right] = iI^{\mathrm{ST}(\pm)}_{z}. \qquad (43)$$

For the symmetries in Table I, the first-order average Hamiltonian in Eq. (39) may be written as follows:

$$\overline{H}^{(1)}_{\mathrm{CS}} = \omega^{\mathrm{ST}}_{\mathrm{nut}}\left(I^{\mathrm{ST}(+)}_{x}\cos\phi_{\mathrm{ST}} + I^{\mathrm{ST}(+)}_{y}\sin\phi_{\mathrm{ST}}\right). \qquad (44)$$

Assume that the density operator of the spin ensemble is prepared with a population difference between the lower triplet state and the singlet state. This arises, for example, if the system is in thermal equilibrium in a strong magnetic field. This state corresponds to a density operator term of the form

$$\rho(0) \sim I^{\mathrm{ST}(+)}_{z}, \qquad (45)$$

omitting numerical factors and orthogonal operators. Suppose that an integer number p of complete RN^{ν}_{n} sequences is applied, with symmetry numbers selected from Table I. The excitation interval is given by $\tau = pT$, where $T = N\tau_R$ is the duration of a complete RN^{ν}_{n} sequence. From the cyclic commutation relationships in Eq. (43), the density operator at the end of the sequence is given by

$$\begin{aligned}\rho(\tau) \simeq\ & I^{\mathrm{ST}(+)}_{z}\cos(\omega^{\mathrm{ST}}_{\mathrm{nut}}\tau) - I^{\mathrm{ST}(+)}_{x}\sin(\omega^{\mathrm{ST}}_{\mathrm{nut}}\tau)\cos(\phi_{\mathrm{ST}})\\ &+ I^{\mathrm{ST}(+)}_{y}\sin(\omega^{\mathrm{ST}}_{\mathrm{nut}}\tau)\sin(\phi_{\mathrm{ST}}). \qquad (46)\end{aligned}$$

This suggests the following phenomena:

1. *Excitation of Singlet–Triplet Coherence.* If the interval τ is chosen such that $\omega^{\mathrm{ST}}_{\mathrm{nut}}\tau$ is approximately an odd multiple of $\pi/2$, the resulting density operator contains terms proportional to the transverse operators $I^{\mathrm{ST}(+)}_{x}$ and $I^{\mathrm{ST}(+)}_{y}$, indicating the excitation of singlet–triplet coherence.[21] In practice, the evolution time τ^{*} is restricted to integer multiples of the basic element duration τ_R. In the absence of dissipative effects, the excitation of a singlet–triplet coherence is optimized by completing the following number of *R*-elements:

$$n^{*} \simeq \mathrm{round}(\pi/(4\omega^{\mathrm{ST}}_{\mathrm{nut}}\tau_{\mathrm{R}})) \quad (\mathrm{ST\ coherence\ excitation}).$$

2. *Generation of Singlet Order.* If the interval τ is chosen such that $\omega_{\rm nut}^{\rm ST}\tau$ is approximately an odd multiple of π, the term $I_z^{\rm ST(+)}$ is inverted in sign. This indicates that the populations of the singlet state and the outer triplet state are swapped. This leads to the generation of singlet order, which is a long-lived difference in the population between the singlet state and the triplet manifold.[1–42] In the absence of relaxation, the conversion of magnetization into singlet-order is optimized by completing the following number of R-elements:

$$n^* \simeq \text{round}(\pi/(2\omega_{\rm nut}^{\rm ST}\tau_{\rm R})) \quad \text{(SO generation)}. \tag{47}$$

It follows that the application of an RN_n^ν sequence to a near-equivalent two-spin-1/2 system in thermal equilibrium leads either to the excitation of singlet–triplet coherences, or to the generation of singlet order, depending on the number of R-elements that are applied. Experimental demonstrations of both effects are given below.

There are technical complications if the number of applied R-elements does not correspond to an integer number of complete RN_n^ν sequences. In such cases, the operators U_J and $U_{\rm rf}$ in Eq. (6) lead to additional transformations. If the total number of completed R-elements is *even*, the main consequence is an additional phase shift of the excited coherences, which is often of little consequence. On the other hand, if the number of applied R-elements is *odd*, then the propagator $U_{\rm rf}$ swaps the $|T_{+1}\rangle$ and $|T_{-1}\rangle$ states, exchanging the $I_z^{\rm ST(\pm)}$ operators.

H. Implementation

1. Standard implementation

The standard implementation of an RN_n^ν sequence is sketched in Fig. 1 and described by Eq. (27).

There is great freedom in the choice of the basic element $\mathscr{R}^0$ upon which the sequence is constructed. In this paper, we concentrate on the implementation shown in Fig. 1, in which the basic element is a three-component composite pulse,[74] with two τ delays inserted between the pulses,

$$\mathscr{R}^0 = (90_{90} - \tau - 180_0 - \tau - 90_{90}), \tag{48}$$

where degrees are used here for the flip angles and the phases. This composite pulse generates an overall rotation by π around the rotating-frame x-axis,[75] and hence is an eligible basic element $\mathscr{R}^0$ for the construction of an RN_n^ν sequence.

The scaling factor κ_{1111}, and hence the nutation frequency of the singlet–triplet transition, depends on the choice of the basic element. In the case of the basic element in Eq. (48), the scaling factor is readily calculated in the limit of "δ-function" pulses, i.e., strong rf pulses with negligible duration. The scaling factors $\kappa_{1\pm11\pm1}$ are given for general N, n, and ν by

$$\kappa_{1\pm11\pm1} = 2^{1/2}\frac{N}{n\pi}(-1)^{(N\pm(n-\nu))/(2N)}\sin^2(n\pi/2N). \tag{49}$$

The scaling factors for a set of RN_n^ν symmetries appropriate for singlet–triplet excitation are given in Table I. The scaling factors with the largest magnitude are offered by sequences with the symmetries R4_3^1, R8_5^1, R8_7^3, and R10_7^2.

Since the scaling factors in Eq. (49) are real, the effective nutation axis of the singlet–triplet transition has a phase angle of zero, $\phi_{\rm ST} = 0$. This result applies to the basic R-element in Eq. (48), in the δ-function pulse limit.

The implementation of an RN_n^ν sequence by the procedure in Fig. 1 provides selective excitation of the transition between the singlet state of a near-equivalent spin-1/2 pair and one of the outer triplet states. However, the sequence performance is not robust with respect to the rf field errors. It is readily shown that a deviation of the rf field from its nominal value induces a net rotation around the z-axis, which accumulates as the sequence proceeds. This causes a degradation in the performance in the case of radiofrequency inhomogeneity or instability.

2. Riffled implementation

In magic-angle-spinning NMR, error compensation is often achieved by the use of supercycles, i.e., repetition of the entire sequence with variations in the phase shifts, or in some cases, cyclic permutations of the pulse sequence elements.[76–80] PulsePol achieves very effective compensation for the rf pulse errors by a much simpler method, namely, a phase shift of just one pulse by 180°. This simple modification may be interpreted as a modified procedure for constructing sequences with RN_n^ν symmetry, but with built-in error compensation.

Consider two different basic elements, denoted here as $\mathscr{R}_A^0$ and $\mathscr{R}_B^0$, as shown in Fig. 3(a). In the depicted case, the two basic elements differ only in that the central 180° pulse is shifted in phase by 180°,

$$\begin{aligned}\mathscr{R}_A^0 &= (90_{90} - \tau - 180_0 - \tau - 90_{90}),\\ \mathscr{R}_B^0 &= (90_{90} - \tau - 180_{180} - \tau - 90_{90}).\end{aligned} \tag{50}$$

Under ideal conditions, both of these basic elements provide a net rotation by an odd multiple of π about the rotating-frame x-axis, and hence are eligible starting points for the RN_n^ν construction procedure. Furthermore, *in the δ-function pulse limit*, the Euler angle trajectories generated by these sequences are identical. This implies that in the case of ideal, infinitely short pulses, the elements $\mathscr{R}_A^0$ and $\mathscr{R}_B^0$ are completely interchangeable. The modified RN_n^ν construction procedure sketched in Fig. 3 exploits this freedom by alternating the phase shifted "A" basic element $(\mathscr{R}_A^0)_{+\pi\nu/N}$ with the phase-shifted conjugate "B" element $(\mathscr{R}_B^{0'})_{-\pi\nu/N}$.

The alternation of two different basic elements, as shown in Fig. 3, resembles the "riffling" technique for shuffling a pack of cards, in which the pack is divided into two piles, and the corners of the two piles are flicked up and released so that the cards intermingle. Therefore, the procedure in Fig. 3 leads to a *riffled* RN_n^ν *sequence*.

Under ideal conditions, and for pulses of infinitesimal duration, the "standard" and "riffled" construction procedures have identical performance. However, an important difference arises in the presence of the rf field amplitude errors. The errors accumulate in the "standard" procedure, but cancel out in the "riffled" procedure. Hence, the procedure shown in Fig. 3 achieves more robust performance with respect to the rf field errors than the standard procedure in Fig. 1. However, it should be emphasized that this form of error compensation does not apply to all basic R-elements, and that even in the current case, strict RN_n^ν symmetry is only maintained in the limit of δ-function pulses. Nevertheless, within these

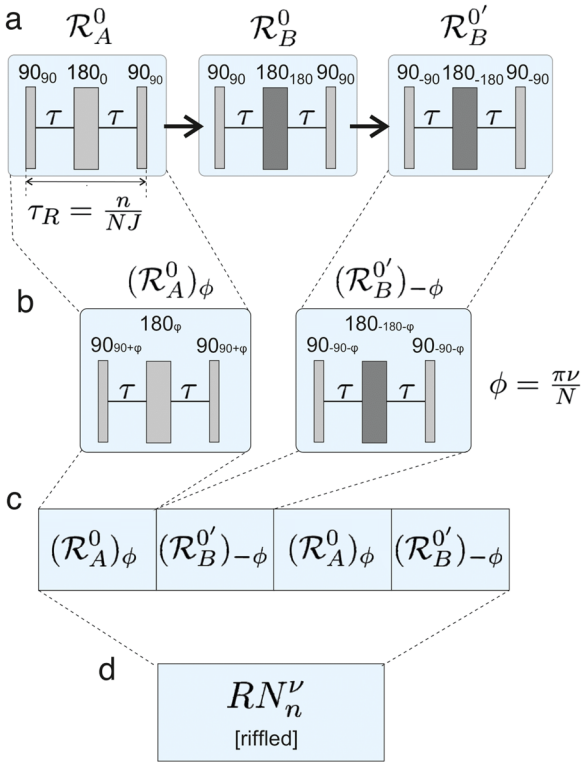

FIG. 3. The construction of a riffled RN_n^ν sequence for singlet–triplet conversion. (a) Two basic *R*-elements are used; the elements $\mathcal{R}_A^0$ and $\mathcal{R}_B^0$ have identical properties under suitable approximations; however, they have opposite responses to pulse imperfections. In the current case, $\mathcal{R}_A^0$ is given by the composite pulse $90_{90}180_0 90_{90}$ with delays τ between the pulses such that its overall duration is $\tau_R = n/(NJ)$. The element $\mathcal{R}_B^0$ is identical but with a 180° phase shift of the central pulse (dark shade). The conjugate sequence $\mathcal{R}_B^{0'}$ is generated from $\mathcal{R}_B^0$ by a change in the sign of all phases. (b) The sequence $\mathcal{R}_A^0$ is given a phase shift of $+\phi$, while the sequence $\mathcal{R}_B^{0'}$ is given a phase shift of $-\phi$, where $\phi = \pi\nu/N$. (c) The pair of sequences $(\mathcal{R}_A^0)_\phi$ and $(\mathcal{R}_B^{0'})_{-\phi}$ is repeated $N/2$ times to give a riffled RN_n^ν sequence (d). PulsePol is an example of a riffled RN_n^ν sequence (see text).

caveats and restrictions, this error-compensation procedure is powerful and useful. As discussed below, error-compensation by riffling is responsible for the robust performance of PulsePol.

To see how a PulsePol sequence[61–63] arises from the riffled RN_n^ν construction procedure, start with the pair of basic *R*-elements given in Eq. (50). Consider the symmetry $R4_3^1$, which is appropriate for transition-selective singlet–triplet excitation, as shown in Table I. This symmetry implies that each *R*-element has duration $\tau_R = (3/4)J^{-1}$ and, hence, that the delays between the pulses are given by $\tau = \tau_R/2 = (3/8)J^{-1}$ in the δ-function pulse limit.

The phase shifts $\pm\pi\nu/N$ are equal to ±45° in the case of $R4_3^1$ symmetry. Hence, the pair of phase-shifted elements is given by

$$\begin{aligned}(\mathscr{R}_A^0)_{+45} &= (90_{135} - \tau - 180_{45} - \tau - 90_{135}),\\ (\mathscr{R}_B^{0'})_{-45} &= (90_{-135} - \tau - 180_{-225} - \tau - 90_{-135}).\end{aligned} \tag{51}$$

This pair of elements may be concatenated, and the pair of elements repeated, to complete the riffled implementation of $R4_3^1$,

$$R4_3^1\,[\text{riffled}] = (\mathscr{R}_A^0)_{+45}(\mathscr{R}_B^{0'})_{-45}(\mathscr{R}_A^0)_{+45}(\mathscr{R}_B^{0'})_{-45}. \tag{52}$$

If the riffled $R4_3^1$ sequence is given a −45° phase shift, we get

$$\begin{aligned}\left[(\mathscr{R}_A^0)_{+45}(\mathscr{R}_B^{0'})_{-45}\right]_{-45} &= (\mathscr{R}_A^0)_0(\mathscr{R}_B^{0'})_{-90}\\ &= 90_{90} - \tau - 180_0 - \tau - 90_{90}\\ &\quad \cdot 90_{-180} - \tau - 180_{-270} - \tau - 90_{-180}.\end{aligned}$$

Adjusting the phases to the range $[0, 360°]$ gives

$$90_{90} - \tau - 180_0 - \tau - 90_{90} \cdot 90_{180} - \tau - 180_{90} - \tau - 90_{180}, \tag{53}$$

which is the version of PulsePol shown in Fig. 3(b) of Ref. 61. The −45° phase shift is of no consequence for the interconversion of singlet order and magnetization.

The riffled construction procedure may be deployed for the other symmetries in Table I. For example, the riffled implementation of $R8_7^3$, using the basic elements in Eq. (50), is as follows:

$$\begin{aligned}R8_7^3\,[\text{riffled}] &= \left[(\mathscr{R}_A^0)_{+67.5}(\mathscr{R}_B^{0'})_{-67.5}\right]^4\\ &= [90_{157.5} - \tau - 180_{67.5} - \tau - 90_{157.5}\\ &\quad \cdot 90_{-157.5} - \tau - 180_{112.5} - \tau - 90_{-157.5}]^4,\end{aligned} \tag{54}$$

where the superscript indicates four repetitions and the interpulse delays are given by $\tau = \tau_R/2 = (7/8)J^{-1}$ in the δ-function pulse limit. Some sequences of this type have been proposed in the form of "generalized PulsePol sequences."[62,63]

The performance of these sequences may be made even more robust by using composite pulses for the 90° or 180° pulse sequence elements.[74,75,81–83] Some examples are demonstrated below.

III. EXPERIMENTAL

A. Sample

Experiments were performed on a solution of a $^{13}C_2$-labeled deutero-alkoxy naphthalene derivative ($^{13}C_2$-DAND), whose molecular structure with its relevant NMR parameters is shown in Table II. Further details of the synthesis of ($^{13}C_2$-DAND) are given in Ref. 84. This compound exhibits a very long $^{13}C_2$ singlet lifetime in low magnetic field.[16] The current experiments were performed on 30 mM of $^{13}C_2$-DAND dissolved in 500 μl isopropanol-d_8. The two ^{13}C sites have a *J*-coupling of 54.39 ± 0.10 Hz and a chemical shift difference of 7.50 ± 0.2 Hz in a magnetic field of 9.39 T. The solution was doped with 3 mM of the paramagnetic agent (2,2,6,6-tetramethylpiperidin-1-yl)oxyl (TEMPO) in order to decrease the T_1 relaxation time, allowing for faster repetition of the experiments, and was contained in a standard Wilmad 5 mM sample tube.

B. NMR equipment

All spectra were acquired at a magnetic field of 9.39 T. A 10 mm NMR probe was used with the radiofrequency amplitude adjusted to give a nutation frequency of $\omega_{nut}/(2\pi) \simeq 12.5$ kHz, corresponding to a 90° pulse duration of 20 μs. It was verified that the signs of

TABLE II. Chemical structure of $^{13}C_2$-DAND (1,2,3,4,5,6,8-heptakis(methoxy-d_3)-7-((propan-2-yl-d_7)oxy)naphthalene-4a,8a-[$^{13}C_2$]) with its relevant NMR parameters in a magnetic field of 9.39 T. The singlet–triplet mixing angle is defined as $\theta_{ST} = \tan^{-1}(\omega_\Delta/2\pi J)$.[24]

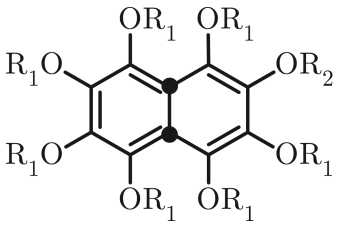

J_{CC}/Hz	54.39 ± 0.10
$\Delta\delta$/ppb	75.0 ± 2.0
$\omega_\Delta/(2\pi)$/Hz [@9.4 T]	7.50 ± 0.20
θ_{ST}/°	7.85 ± 0.22

radiofrequency phase shifts correspond to the rotating-frame Hamiltonian in Eq. (4), taking into account the sense of precession and the radiofrequency mixing scheme.[85,86]

C. Pulse sequences

1. Singlet–triplet excitation

The excitation of coherences between the singlet state and the outer triplet states of $^{13}C_2$-DAND was demonstrated using the pulse sequence in Fig. 4(a). On each transient, a singlet destruction block[20] is applied followed by a waiting time of ~5T_1 to establish thermal equilibrium. This ensures an initial condition free from interference by residual long-lived singlet order left over from the previous transient. After thermal equilibration in the magnetic field, an RN_n^ν symmetry-based singlet–triplet excitation sequence of duration τ_{exc} is applied, and the NMR signal is detected immediately afterward. Fourier transformation of the signal generates the ^{13}C NMR spectrum.

2. Singlet order generation

The generation of singlet order is assessed by the pulse sequence scheme in Fig. 4(b). After the destruction of residual singlet order and thermal equilibration, an M2S or an RN_n^ν sequence of duration τ_{exc} is applied to generate singlet order. This is followed by a T_{00}

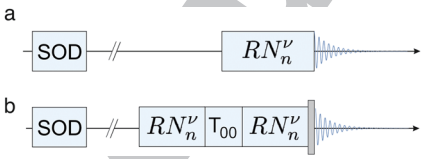

FIG. 4. High-field NMR pulse sequences used in this work. (a) After a singlet-order destruction sequence (SOD)[20] and a waiting interval to establish thermal equilibrium, an RN_n^ν sequence is applied to thermal equilibrium magnetization, exciting coherences between the singlet state and one of the outer triplet states. (b) Procedure for estimating singlet order generation. An RN_n^ν sequence is applied to generate singlet order, followed by a T_{00} singlet-order-filtering sequence,[8,87] and a second RN_n^ν sequence to regenerate z-magnetization. The NMR signal is induced by applying a composite 90° pulse (grey rectangle).

singlet filter sequence.[6] This consists of a sequence of rf pulses and pulsed field gradients that dephase all signal components not associated with nuclear singlet order. The singlet order is reconverted to z-magnetization by a second RN_n^ν sequence of equal duration to the first, or by an S2M sequence (time-reverse of the M2S sequence).[5,6] The recovered z-magnetization is converted to transverse magnetization by a composite 90° pulse, and the NMR signal is detected in the following interval. The signal amplitude serves as a measure of the singlet order generated by the excitation sequence, and the efficiency of recovering magnetization from the singlet order. The maximum theoretical efficiency for passing magnetization through singlet order is 2/3.[88]

The RN_n^ν sequences may be constructed by either the standard or the riffled procedures. M2S and S2M sequences may be substituted for the first and last RN_n^ν sequences, respectively. The 90° readout pulse in Fig. 4(b) was implemented as a symmetrized BB1 composite pulse.[89,90] The details of the composite pulse, the SOD sequence, and the T_{00} pulse sequence modules are given in the supplementary material.

IV. RESULTS

A. Transition-selective singlet–triplet excitation

In systems of near-equivalent spin-1/2 pairs, the chemical shift difference induces a slight mixing of the singlet state $|S_0\rangle$ with the central triplet state $|T_0\rangle$. This effect lends signal intensity to the single-quantum coherences between the singlet state and the outer triplet states $|T_{\pm1}\rangle$, which generate the outer lines of the AB quartet. These peaks are feeble for two independent reasons: (i) the coupling of the singlet–triplet coherences to observable transverse magnetization is weak in the near-equivalence limit, and (ii) the singlet–triplet coherences are excited only weakly by conventional single-pulse excitation. The first of these factors is an intrinsic property of a singlet–triplet coherence. On the other hand, the second factor may be overcome by using a suitable excitation sequence to generate the desired coherence with full amplitude. Many such schemes have been devised.[21] This effect is useful since the frequencies of these peaks provide an accurate estimate of the internuclear J-coupling, which can be difficult to estimate in the near-equivalence regime.

Figure 5(a) shows the ^{13}C NMR spectrum of the $^{13}C_2$-DAND solution. The strong central doublet is due to the two triplet–triplet coherences. The outer peaks of the AB quartet, which correspond to the weakly allowed singlet–triplet coherences, are barely visible in the spectrum, even after vertical expansion [Fig. 5(b)].

Greatly enhanced excitation of the outer AB peaks is achieved by the pulse sequence in Fig. 4(a) using an excitation sequence of symmetry $R4_3^1$ constructed by the riffled procedure (Fig. 3) and with the number of R-elements satisfying Eq. (47). The strong enhancement of the outer AB peaks, relative to the spectrum induced by a single 90° pulse, is self-evident in Fig. 5(c). Note that changing the sign of the symmetry number ν switches the excitation to the opposite singlet–triplet transition [Fig. 5(d)]. The experimental pulse sequence parameters are given in Table III.

In the high-temperature limit, the sign of the J-coupling makes no difference to the appearance of the spectrum since changing the sign of J simultaneously swaps the outer triplet state that the singlet state is coupled to and the spectral frequencies of the

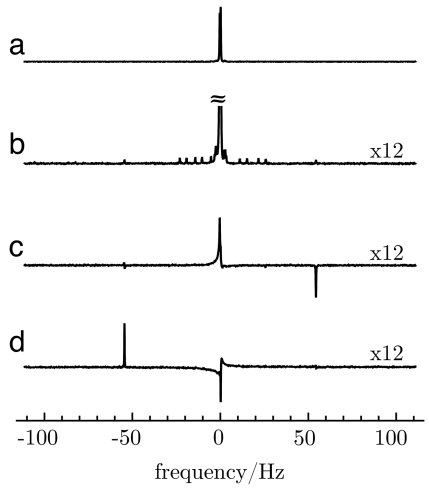

FIG. 5. Enhanced singlet–triplet coherent excitation. (a) Conventional ^{13}C spectrum of $^{13}C_2$-DAND using a single 90° pulse for excitation, showing strong signals from the triplet–triplet coherences. (b) Vertical expansion (by a factor of 12) of the conventional ^{13}C spectrum. Additional signals are visible from minority isotopomers, with the outer peaks barely visible. The strong central peak is truncated. (c) Spectrum obtained by applying four elements of a riffled $R4_3^1$ sequence, showing a strongly enhanced outer peak. The construction procedure in Fig. 3 was used, starting from the basic elements in Eq. (50). (d) Spectrum obtained by applying four elements of an $R4_3^{-1}$ sequence, showing the enhancement of the other outer peak. All spectra were obtained with a total of 256 transients and the same processing parameters. No line broadening is applied.

TABLE III. Experimental parameters for the $R4_3^{\pm 1}$ sequences used to obtain the results in Figs. 5(c) and 5(d). The parameters have the following meaning: ω_{nut} is the radiofrequency pulse amplitude, expressed as a nutation frequency; τ_{90} is the duration of a 90° pulse; τ_R is the duration of a single *R*-element; τ is the interval between pulses within each *R*-element (see Fig. 1); n_R^{exc} is the number of *R*-elements in the excitation sequence; τ_{exc} is the duration of the excitation sequence.

$\omega_{nut}/(2\pi)$	12.5 kHz
τ_{90}	20 μs
τ_R	13 800 μs
τ	6860 μs
n_R^{exc}	4
τ_{exc}	55.2 ms

excited singlet–triplet transition. The more complex behavior in hyperpolarized spin systems will be discussed in a future paper.

B. Magnetization-to-singlet conversion

The experimental performance of some magnetization-to-singlet conversion schemes was tested on a TEMPO-doped solution of $^{13}C_2$-DAND by using the pulse sequence protocol in Fig. 4(b). A selection of singlet-filtered NMR spectra is shown in Figs. 6(b)–6(f). In all cases, the pulse sequence parameters were optimized for the best performance. The optimized parameters are given in the supplementary material.

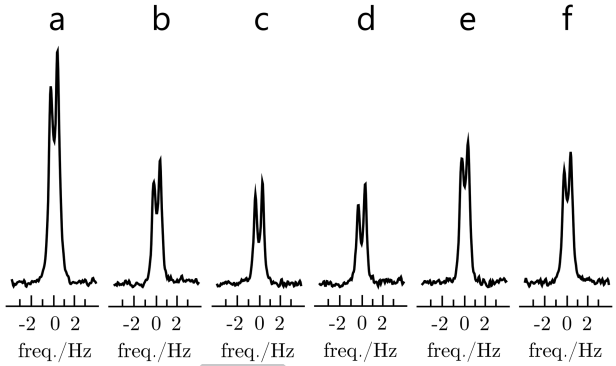

FIG. 6. ^{13}C spectra obtained after (a) a single 90° pulse, or (b)–(f) after filtering the ^{13}C NMR signal through singlet order by using the scheme in Fig. 4(b). (a) Standard ^{13}C spectrum obtained with a single 90° pulse. (b) Singlet-filtered spectrum obtained with M2S for singlet order excitation and S2M for reconversion to magnetization. (c) Singlet-filtered spectrum obtained with a pair of $R4_3^1$ sequences. (d) Singlet-filtered spectrum obtained with a pair of $R8_7^3$ sequences. Both (c) and (d) use the standard implementation of RN_n^ν sequences, as in Fig. 1, using the basic element in Eq. (48). (e) Singlet-filtered spectrum obtained with a pair of riffled $R4_3^1$ sequences. (f) Singlet-filtered spectrum obtained with a pair of riffled $R8_7^3$ sequences. Both (e) and (f) use the riffled implementation of RN_n^ν sequences, as in Fig. 3, using the basic elements in Eq. (50). All pulse sequence parameters are given in the supplementary material.

Figure 6(a) shows the unfiltered ^{13}C NMR spectrum of $^{13}C_2$-DAND. The different linewidths of the two doublet components are due to the cross-correlation of the fluctuating dipole–dipole and chemical shift anisotropy interactions.[91]

Figure 6(b) shows the spectrum obtained by applying an M2S sequence to generate singlet order, suppressing other spin order terms, and regenerating magnetization from singlet order by applying an S2M sequence. Approximately 50% of the spin order is lost by this procedure, as may be seen by comparing the spectra in Figs. 6(a) and 6(b). The theoretical limit on passing magnetization through singlet order is $2/3 \simeq 67\%$.

The results obtained by using RN_n^ν sequences with different sets of symmetry numbers are shown in Figs. 6(c) and 6(d). The standard RN_n^ν construction procedure in Fig. 1 was used. The number of *R*-elements was selected according to Eq. (47). The results are slightly inferior to the M2S sequence. Some of these spectra exhibit perturbed peak intensities. This is unexplained.

Riffled RN_n^ν sequences constructed by the procedure in Fig. 3 display an improved performance, which is distinctly superior to M2S, as shown in Figs. 6(e) and 6(f). The improvement is attributed to the increased robustness of the riffled procedure with respect to a range of experimental imperfections, as discussed further below.

Note that the riffled $R4_3^1$ sequence only differs from PulsePol[61–63] by an overall phase shift [Eq. (52) and (53)]. The increased robustness of PulsePol with respect to M2S/S2M in the context of singlet/triplet conversion has been anticipated by the simulations of Tratzmiller.[62]

The singlet order relaxation time T_S is readily estimated by introducing a variable delay before the second RN_n^ν sequence in Fig. 4(b). Some results are shown in the supplementary material. The estimated relaxation time constants are $T_S = 89.4 \pm 4.3$ s and

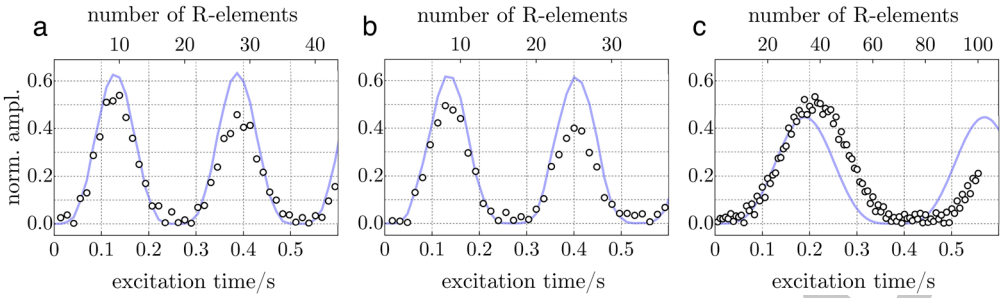

FIG. 7. Experimental ^{13}C signal amplitudes (white dots) for the protocol in Fig. 4(b) using riffled RN_n^ν sequences for both the excitation and reconversion of singlet order. The following symmetries were used: (a) $R4_3^1$, (b) $R8_7^3$, and (c) $R10_3^2$. The number n_R of R-elements in the RN_n^ν sequences for singlet excitation and reconversion is varied simultaneously (top horizontal axis). The corresponding total duration of each sequence is shown on the lower horizontal axis. All sequences were implemented by the riffled procedure in Fig. 3 using the basic elements in Eq. (50). The signal amplitudes are normalized relative to that generated by a single 90° pulse. Light blue trajectories show numerical simulations (excluding relaxation) with the pulse sequence parameters given in the supplementary material.

$T_1 = 3.41 \pm 0.05$ s. Although T_S is much larger than T_1, the relaxation of singlet order is faster than that observed in previous experiments.[16] This is attributed to the TEMPO doping of the solution in the current case.

Figure 7 shows the dependence of the singlet-filtered NMR signals on the number of R-elements n_R, used for both the excitation and reconversion sequence. The corresponding total sequence durations $\tau_{exc} = \tau_{recon} = n_R\tau_R = n_R(n/N)J^{-1}$ are also shown. Clear oscillations of the singlet order are observed, as predicted by Eq. (46). The singlet order oscillations induced by $R8_7^3$ are slightly slower than those for $R4_3^1$, as expected from the theoretical scaling factors reported in Table I. The $R10_3^2$ sequence induces a relatively slow oscillation, corresponding to the small value of κ_{1111} for this symmetry. In all cases, numerical simulations by *SpinDynamica* software[92] show qualitative agreement with the experimental results.

The improved robustness of the riffled implementation of RN_n^ν with respect to the rf amplitude variations is illustrated by the experimental results in Fig. 8. These plots show the singlet-filtered signal amplitudes as a function of the rf field amplitude by using the protocol in Fig. 4(b). Two different pulse sequence symmetries are explored: $R4_3^1$ (blue, left column) and $R8_7^3$ (red, right column). The horizontal axis represents the rf field amplitude expressed as a nutation frequency ω_{nut}. The horizontal coordinates are given by the ratio $\omega_{nut}/\omega_{nut}^0$, where the nominal nutation frequency ω_{nut}^0 is used to calculate the pulse durations, which are kept fixed. Row a shows that the $R4_3^1$ and $R8_7^3$ sequences are both fairly narrowband with respect to the rf field amplitude when the standard RN_n^ν protocol is used (Fig. 1). Row b shows that their robustness with respect to rf amplitude errors is greatly improved by the riffled variant of the RN_n^ν protocol, inspired by PulsePol (Fig. 3). Their tolerance of rf amplitude errors is increased further when the central 180° pulses of the basic R-elements are replaced by ASBO-11 composite pulses[83] (row c). The use of $60_{180}180_0240_{180}420_0240_{180}180_060_{180}$ composite pulses[82] provides less improvement (row d). For comparison, the experimental performance of the M2S/S2M protocol[5,6] is shown by the grey lines in row d. The performance of M2S/S2M is clearly inferior to that of the riffled RN_n^ν sequences.

Another important characteristic of pulse sequences for the generation and reconversion of singlet order is their robustness with

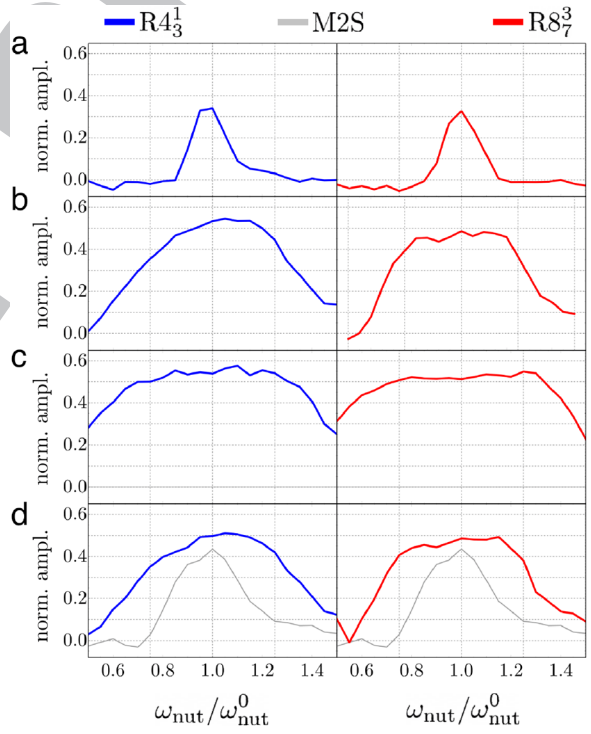

FIG. 8. Experimental ^{13}C signal amplitudes of $^{13}C_2$-DAND solution, obtained by the protocol in Fig. 4(b), as a function of relative nutation frequency $\omega_{nut}/\omega_{nut}^0$, where ω_{nut}^0 represents the nominal nutation frequency used for the calculation of pulse durations. The traces correspond to the experimental amplitudes for converting magnetization into singlet order and back again, normalized with respect to the signal generated by a single 90° pulse. Left column (blue): $R4_3^1$ sequences. Right column (red): $R8_7^3$ sequences. (a) Standard RN_n^ν sequences using the basic element in Eq. (48). (b) Riffled RN_n^ν sequences using the basic elements in Eq. (50). (c) Riffled RN_n^ν sequences with all central 180_0 pulses replaced by an ASBO-11 composite pulse.[83] (d) Riffled RN_n^ν sequences with all central 180_0 pulses replaced by a $60_{180}180_0240_{180}420_0240_{180}180_060_{180}$ composite pulse.[82] The grey lines in (d) show the experimental response of the M2S/S2M protocol. All experimental details are given in the supplementary material.

respect to resonance offset, defined here as $\Delta\omega = \frac{1}{2}\omega_\Sigma$, where ω_Σ is the sum of the chemically shifted offset frequencies [see Eq. (3)]. A robust performance with respect to resonance offset is usually desirable since it renders the sequence less sensitive to inhomogeneity in the static magnetic field, which can be particularly important in low-field applications.

Figure 9 compares the resonance-offset dependence of several pulse sequences for the generation and reconversion of $^{13}C_2$ singlet order in the solution of $^{13}C_2$-DAND. The left column compares different schemes that have $R4_3^1$ symmetry. The right column compares different schemes that have $R8_7^3$ symmetry. All experimental parameters are given in the supplementary material.

Figure 9(a) shows the resonance-offset dependence of RN_n^ν sequences constructed by the standard protocol of Fig. 1 using the basic R-element of Eq. (48). The resulting sequences have a strong dependence on resonance offset, with the $R8_7^3$ sequence displaying a particularly undesirable offset dependence.

Figure 9(b) shows the resonance-offset dependence of riffled RN_n^ν sequences using the pair of basic R-elements in Eq. (50). Riffling clearly stabilizes the resonance offset dependence, with the improvement being particularly striking for $R8_7^3$.

Figures 9(c) and 9(d) explore the effect of substituting the central 180° pulse of the basic R-elements with composite pulses. Although ASBO-11 composite pulses[83] do not change the performance of $R4_3^1$ very much, they do lead to a significant increase in the bandwidth of $R8_7^3$ [Fig. 9(c)]. An even more pronounced effect is observed upon replacing all single 180° pulses with seven-element $60_{180}180_0240_{180}420_0240_{180}180_060_{180}$ composite pulses[82] [Fig. 9(d)]. The resonance-offset bandwidth of $R8_7^3$ with seven-element composite pulses[82] is particularly impressive.

The gray lines in Fig. 9(d) show the experimental offset dependence of the M2S/S2M protocol.[5] All riffled RN_n^ν sequences have clearly superior performance to M2S/S2M. To put this in context, even the M2S/S2M protocol is regarded as relatively robust with respect to the resonance offset, being first demonstrated on a sample in an inhomogeneous low magnetic field.[5] Some other techniques, such as SLIC,[9] are far more sensitive to the resonance offset than M2S.

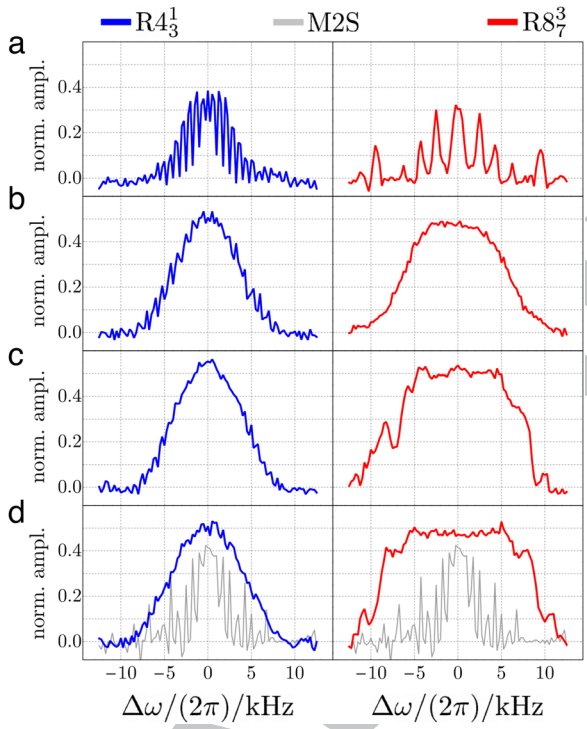

FIG. 9. Experimental ^{13}C signal amplitudes of $^{13}C_2$-DAND solution, obtained by the protocol in Fig. 4(b), as a function of resonance offset $\Delta\omega$. The plotted points correspond to the amplitude for converting magnetization into singlet order and back again, normalized with respect to the signal generated by a single 90° pulse. Left column (blue): $R4_3^1$ sequences. Right column (red): $R8_7^3$ sequences. (a) Standard RN_n^ν sequences using the basic element in Eq. (48). (b) Riffled RN_n^ν sequences using the basic elements in Eq. (50). (c) Riffled RN_n^ν sequences with all central 180_0 pulses replaced by an ASBO-11 composite pulse.[83] (d) Riffled RN_n^ν sequences with all central 180_0 pulses replaced by a $60_{180}180_0240_{180}420_0240_{180}180_060_{180}$ composite pulse.[82] The grey lines in (d) show the experimental response of the M2S/S2M protocol. All experimental details are given in the supplementary material.

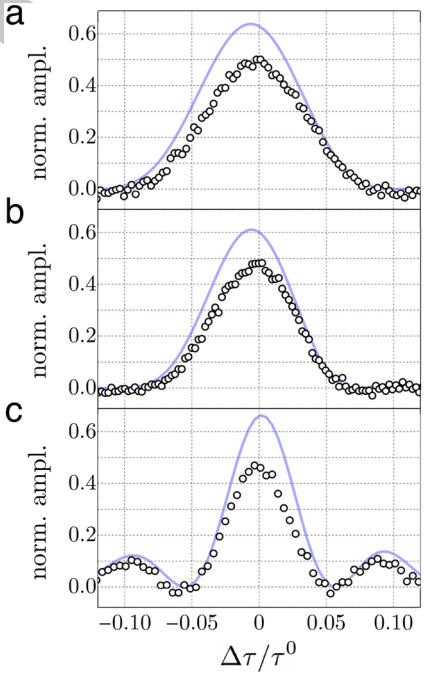

FIG. 10. Experimental ^{13}C signal amplitudes (white dots) for (a) $R4_3^1$, (b) $R8_7^3$, and (c) M2S as a function of the relative inter-pulse delay mismatch $\Delta\tau/\tau^0$, where τ^0 represents the nominal inter-pulse delay. For the M2S sequence, the nominal inter-pulse delay is given by $\tau^0 = 1/(4J)$, whereas for R-based sequences, the nominal inter-pulse delay is given by $\tau^0 = n/(NJ)$ (neglecting pulse durations in both cases). The R-sequences were implemented using the riffled procedure in Fig. 3. The final ^{13}C signal amplitudes were referenced with respect to a single ^{13}C pulse-acquire spectrum. Light blue trajectories represent the numerical simulations with the pulse sequence parameters given in the supplementary material. Relaxation was neglected in all cases.

The results for the dependence of the singlet order conversion on the pulse sequence intervals are shown in Fig. 10. Both the $R4_3^1$ and $R8_7^3$ sequences display an improved tolerance to misset of the pulse sequence intervals compared to M2S.

V. DISCUSSION

The results shown in this paper indicate that PulsePol is a very attractive addition to the arsenal of pulse sequences for the manipulation of nuclear singlet order. The PulsePol sequences provide a high degree of robustness with respect to common experimental imperfections, which is found to be superior to the existing methods such as M2S/S2M, especially when combined with composite pulses. This robustness is likely to be particularly important for applications to imaging and *in vivo* experiments.[25,35]

In addition, PulsePol is a relatively simple repeating sequence of six pulses. This structure has many advantages over M2S, which performs the magnetization-to-singlet-order transformation in four consecutive steps.[5,6] For example, the PulsePol repetitions may be stopped at any time in order to achieve a partial transformation of spin order. This is more difficult to achieve for M2S and its variants.

The theoretical relationship between PulsePol and symmetry-based recoupling sequences in solid-state NMR is unexpected. Nevertheless, this theoretical analogy immediately allows the considerable body of average Hamiltonian theory developed for symmetry-based recoupling to be deployed in this very different context. This immediately allows the use of symmetry-based selection rules for analyzing the existing PulsePol sequences and for designing new variants.

All of the work reported in this paper uses the same set of basic elements given in Eqs. (48) and (50). There is clearly scope for using different basic elements within the RN_n^ν symmetry framework.

As discussed above, PulsePol may be interpreted as a variant implementation of RN_n^ν symmetry involving the alternation of two different basic elements, which compensate each other's imperfections. Such riffled RN_n^ν sequences are more robust with respect to a range of experimental imperfections. The same principle might be applied to symmetry-based recoupling sequences in magic-angle-spinning solids. Extensions are also possible, involving more complex interleaved patterns of multiple basic elements. We intend to explore such "riffled supercycles" in future work.

In magic-angle-spinning solid-state NMR, symmetry-based pulse sequences have been used to address a wide variety of spin dynamical problems,[64–67] including multiple-channel sequences for the recoupling of heteronuclear systems.[63,67] Such extensions should be possible in the solution NMR context as well.

Variants of M2S/S2M sequences have been applied to heteronuclear spin systems.[36–38] This has important applications in parahydrogen-induced polarization.[36] It is likely that riffled RN_n^ν sequences are also applicable to this problem.

The theory of symmetry-based recoupling in magic-angle-spinning solids was originally formulated by using average Hamiltonian theory, as sketched above. It is also possible to obtain the key results using Floquet theory,[93,94] which may have advantages in certain circumstances. Floquet theory should also be applicable to the current context.

In summary, the PulsePol sequence[61–63] is an important innovation that has potential applications in many forms of magnetic resonance. It sits at the fertile intersection of diamond magnetometry, quantum information processing, solid-state NMR, parahydrogen-induced hyperpolarization, and singlet NMR in solution.

SUPPLEMENTARY MATERIAL

The supplementary material includes further experimental details on the implementation of the composite pulses, the M2S sequence, the T_{00} filter, the SOD filter, and the experiments measuring the T_1 and T_S relaxation times.

ACKNOWLEDGMENTS

We acknowledge funding received by the European Research Council (Grant No. 786707-FunMagResBeacons) and EPSRC-UK (Grant Nos. EP/P009980/1, EP/P030491/1, and EP/V055593/1). We thank Sami Jannin, Quentin Stern, Chloé Gioiosa, Olivier Cala, Laurynas Dagys, Stuart J. Elliott, and Maria Concistré for help and discussions.

AUTHOR DECLARATIONS

Conflict of Interest

The authors have no conflicts to disclose.

Author Contributions

Mohamed Sabba: Conceptualization (lead); Data curation (lead); Formal analysis (equal); Investigation (lead); Methodology (lead); Project administration (equal); Resources (equal); Validation (lead); Visualization (supporting); Writing – original draft (equal); Writing – review & editing (equal). **Nino Wili**: Conceptualization (lead); Formal analysis (supporting); Methodology (equal); Writing – original draft (equal); Writing – review & editing (equal). **Christian Bengs**: Conceptualization (equal); Data curation (equal); Formal analysis (equal); Methodology (equal); Software (lead); Visualization (lead); Writing – original draft (equal); Writing – review & editing (equal). **James W. Whipham**: Formal analysis (equal). **Lynda J. Brown**: Methodology (equal); Resources (lead); Supervision (equal); Writing – original draft (equal); Writing – review & editing (equal). **Malcolm H. Levitt**: Conceptualization (equal); Funding acquisition (lead); Project administration (lead); Resources (lead); Supervision (lead); Visualization (equal); Writing – original draft (equal); Writing – review & editing (equal).

DATA AVAILABILITY

The data that support the findings of this study are available from the corresponding author upon reasonable request.

REFERENCES

[1] *Long-Lived Nuclear Spin Order: Theory and Applications*, 1st ed., edited by G. Pileio (Royal Society of Chemistry, S.l., 2020).

[2] M. Carravetta, O. G. Johannessen, and M. H. Levitt, "Beyond the T_1 limit: Singlet nuclear spin states in low magnetic fields," Phys. Rev. Lett. **92**, 153003 (2004).

[3] M. Carravetta and M. H. Levitt, "Long-lived nuclear spin states in high-field solution NMR," J. Am. Chem. Soc. **126**, 6228–6229 (2004).

[4] R. Sarkar, P. R. Vasos, and G. Bodenhausen, "Singlet-state exchange NMR spectroscopy for the study of very slow dynamic processes," J. Am. Chem. Soc. **129**, 328–334 (2007).

[5] G. Pileio, M. Carravetta, and M. H. Levitt, "Storage of nuclear magnetization as long-lived singlet order in low magnetic field," Proc. Natl. Acad. Sci. U. S. A. **107**, 17135–17139 (2010).

[6] M. C. D. Tayler and M. H. Levitt, "Singlet nuclear magnetic resonance of nearly-equivalent spins," Phys. Chem. Chem. Phys. **13**, 5556–5560 (2011).

[7] M. H. Levitt, "Singlet nuclear magnetic resonance," Annu. Rev. Phys. Chem. **63**, 89–105 (2012).

[8] M. C. D. Tayler and M. H. Levitt, "Accessing long-lived nuclear spin order by isotope-induced symmetry breaking," J. Am. Chem. Soc. **135**, 2120–2123 (2013).

[9] S. J. DeVience, R. L. Walsworth, and M. S. Rosen, "Preparation of nuclear spin singlet states using spin-lock induced crossing," Phys. Rev. Lett. **111**, 173002 (2013).

[10] S. J. DeVience, "Nuclear magnetic resonance with spin singlet states and nitrogen vacancy centers in diamond," Ph.D. thesis, Harvard University, Massachusetts, 2014.

[11] S. J. DeVience, R. L. Walsworth, and M. S. Rosen, "Probing scalar coupling differences via long-lived singlet states," J. Magn. Reson. **262**, 42–49 (2016).

[12] S. J. DeVience, M. Greer, S. Mandal, and M. S. Rosen, "Homonuclear J-coupling spectroscopy at low magnetic fields using spin-lock induced crossing," ChemPhysChem **22**, 2128–2137 (2021).

[13] M. H. Levitt, "Long live the singlet state!," J. Magn. Reson. **306**, 69–74 (2019).

[14] Y. Zhang, P. C. Soon, A. Jerschow, and J. W. Canary, "Long-lived ^{1}H nuclear spin singlet in dimethyl maleate revealed by addition of thiols," Angew. Chem., Int. Ed. **53**, 3396–3399 (2014).

[15] Y. Zhang, K. Basu, J. W. Canary, and A. Jerschow, "Singlet lifetime measurements in an all-proton chemically equivalent spin system by hyperpolarization and weak spin lock transfers," Phys. Chem. Chem. Phys. **17**, 24370–24375 (2015).

[16] G. Stevanato, J. T. Hill-Cousins, P. Håkansson, S. S. Roy, L. J. Brown, R. C. D. Brown, G. Pileio, and M. H. Levitt, "A nuclear singlet lifetime of more than one hour in room-temperature solution," Angew. Chem., Int. Ed. **54**, 3740–3743 (2015).

[17] A. N. Pravdivtsev, A. S. Kiryutin, A. V. Yurkovskaya, H.-M. Vieth, and K. L. Ivanov, "Robust conversion of singlet spin order in coupled spin-1/2 pairs by adiabatically ramped RF-fields," J. Magn. Reson. **273**, 56–64 (2016).

[18] B. A. Rodin, A. S. Kiryutin, A. V. Yurkovskaya, K. L. Ivanov, S. Yamamoto, K. Sato, and T. Takui, "Using optimal control methods with constraints to generate singlet states in NMR," J. Magn. Reson. **291**, 14–22 (2018).

[19] B. A. Rodin, V. P. Kozinenko, A. S. Kiryutin, A. V. Yurkovskaya, J. Eills, and K. L. Ivanov, "Constant-adiabaticity pulse schemes for manipulating singlet order in 3-spin systems with weak magnetic non-equivalence," J. Magn. Reson. **327**, 106978 (2021).

[20] B. A. Rodin, K. F. Sheberstov, A. S. Kiryutin, L. J. Brown, R. C. D. Brown, M. Sabba, M. H. Levitt, A. V. Yurkovskaya, and K. L. Ivanov, "Fast destruction of singlet order in NMR experiments," J. Chem. Phys. **151**, 234203 (2019).

[21] K. F. Sheberstov, A. S. Kiryutin, C. Bengs, J. T. Hill-Cousins, L. J. Brown, R. C. D. Brown, G. Pileio, M. H. Levitt, A. V. Yurkovskaya, and K. L. Ivanov, "Excitation of singlet–triplet coherences in pairs of nearly-equivalent spins," Phys. Chem. Chem. Phys. **21**, 6087–6100 (2019).

[22] B. Kharkov, X. Duan, E. S. Tovar, J. W. Canary, and A. Jerschow, "Singlet excitation in the intermediate magnetic equivalence regime and field-dependent study of singlet–triplet leakage," Phys. Chem. Chem. Phys. **21**, 2595–2600 (2019).

[23] S. Mamone, N. Rezaei-Ghaleh, F. Opazo, C. Griesinger, and S. Glöggler, "Singlet-filtered NMR spectroscopy," Sci. Adv. **6**, eaaz1955 (2020).

[24] C. Bengs, M. Sabba, A. Jerschow, and M. H. Levitt, "Generalised magnetisation-to-singlet-order transfer in nuclear magnetic resonance," Phys. Chem. Chem. Phys. **22**, 9703–9712 (2020).

[25] S. Mamone, A. B. Schmidt, N. Schwaderlapp, T. Lange, D. von Elverfeldt, J. Hennig, and S. Glöggler, "Localized singlet-filtered MRS in vivo," NMR Biomed. **34**, e4400 (2021).

[26] C. Bengs, L. Dagys, G. A. I. Moustafa, J. W. Whipham, M. Sabba, A. S. Kiryutin, K. L. Ivanov, and M. H. Levitt, "Nuclear singlet relaxation by chemical exchange," J. Chem. Phys. **155**, 124311 (2021).

[27] S. Cavadini, J. Dittmer, S. Antonijevic, and G. Bodenhausen, "Slow diffusion by singlet state NMR spectroscopy," J. Am. Chem. Soc. **127**, 15744–15748 (2005).

[28] S. Cavadini and P. R. Vasos, "Singlet states open the way to longer time-scales in the measurement of diffusion by NMR spectroscopy," Concepts Magn. Reson., Part A **32**, 68–78 (2008).

[29] R. Sarkar, P. Ahuja, P. R. Vasos, and G. Bodenhausen, "Measurement of slow diffusion coefficients of molecules with arbitrary scalar couplings via long-lived spin states," ChemPhysChem **9**, 2414–2419 (2008).

[30] P. Ahuja, R. Sarkar, P. R. Vasos, and G. Bodenhausen, "Diffusion coefficients of biomolecules using long-lived spin states," J. Am. Chem. Soc. **131**, 7498–7499 (2009).

[31] N. Salvi, R. Buratto, A. Bornet, S. Ulzega, I. Rentero Rebollo, A. Angelini, C. Heinis, and G. Bodenhausen, "Boosting the sensitivity of ligand–protein screening by NMR of long-lived states," J. Am. Chem. Soc. **134**, 11076–11079 (2012).

[32] R. Buratto, D. Mammoli, E. Chiarparin, G. Williams, and G. Bodenhausen, "Exploring weak ligand–protein interactions by long-lived NMR states: Improved contrast in fragment-based drug screening," Angew. Chem., Int. Ed. **53**, 11376–11380 (2014).

[33] R. Buratto, A. Bornet, J. Milani, D. Mammoli, B. Vuichoud, N. Salvi, M. Singh, A. Laguerre, S. Passemard, S. Gerber-Lemaire, S. Jannin, and G. Bodenhausen, "Drug screening boosted by hyperpolarized long-lived states in NMR," ChemMedChem **9**, 2509–2515 (2014).

[34] R. Buratto, D. Mammoli, E. Canet, and G. Bodenhausen, "Ligand–protein affinity studies using long-lived states of fluorine-19 nuclei," J. Med. Chem. **59**, 1960–1966 (2016).

[35] S. Berner, A. B. Schmidt, M. Zimmermann, A. N. Pravdivtsev, S. Glöggler, J. Hennig, D. von Elverfeldt, and J. B. Hövener, "SAMBADENA hyperpolarization of ^{13}C-succinate in an MRI: Singlet-triplet mixing causes polarization loss," ChemistryOpen **8**, 728–736 (2019).

[36] J. Eills, G. Stevanato, C. Bengs, S. Glöggler, S. J. Elliott, J. Alonso-Valdesueiro, G. Pileio, and M. H. Levitt, "Singlet order conversion and parahydrogen-induced hyperpolarization of ^{13}C nuclei in near-equivalent spin systems," J. Magn. Reson. **274**, 163–172 (2017).

[37] G. Stevanato, J. Eills, C. Bengs, and G. Pileio, "A pulse sequence for singlet to heteronuclear magnetization transfer: S2hM," J. Magn. Reson. **277**, 169–178 (2017).

[38] C. Bengs, L. Dagys, and M. H. Levitt, "Robust transformation of singlet order into heteronuclear magnetisation over an extended coupling range," J. Magn. Reson. **321**, 106850 (2020).

[39] D. E. Korenchan, J. Lu, M. H. Levitt, and A. Jerschow, "^{31}P nuclear spin singlet lifetimes in a system with switchable magnetic inequivalence: Experiment and simulation," Phys. Chem. Chem. Phys. **23**, 19465–19471 (2021).

[40] B. Kharkov, X. Duan, J. Rantaharju, M. Sabba, M. H. Levitt, J. W. Canary, and A. Jerschow, "Weak nuclear spin singlet relaxation mechanisms revealed by experiment and computation," Phys. Chem. Chem. Phys. **24**, 7531–7538 (2022).

[41] S. S. Roy and T. S. Mahesh, "Initialization of NMR quantum registers using long-lived singlet states," Phys. Rev. A **82**, 052302 (2010).

[42] B. A. Rodin, C. Bengs, A. S. Kiryutin, K. F. Sheberstov, L. J. Brown, R. C. D. Brown, A. V. Yurkovskaya, K. L. Ivanov, and M. H. Levitt, "Algorithmic cooling of nuclear spins using long-lived singlet order," J. Chem. Phys. **152**, 164201 (2020).

[43] C. R. Bowers and D. P. Weitekamp, "Parahydrogen and synthesis allow dramatically enhanced nuclear alignment," J. Am. Chem. Soc. **109**, 5541–5542 (1987).

[44] M. G. Pravica and D. P. Weitekamp, "Net NMR alignment by adiabatic transport of parahydrogen addition products to high magnetic field," Chem. Phys. Lett. **145**, 255–258 (1988).

[45] S. Kadlecek, K. Emami, M. Ishii, and R. Rizi, "Optimal transfer of spin-order between a singlet nuclear pair and a heteronucleus," J. Magn. Reson. **205**, 9–13 (2010).

[46] L. Dagys, C. Bengs, and M. H. Levitt, "Low-frequency excitation of singlet–triplet transitions. Application to nuclear hyperpolarization," J. Chem. Phys. **155**, 154201 (2021).

[47] L. Dagys and C. Bengs, "Hyperpolarization read-out through rapidly rotating fields in the zero- and low-field regime," Phys. Chem. Chem. Phys. **24**, 8321–8328 (2022).

[48] C. Huang, Y. Peng, E. Lin, Z. Ni, X. Lin, H. Zhan, Y. Huang, and Z. Chen, "Adaptable singlet-filtered nuclear magnetic resonance spectroscopy for chemical and biological applications," Anal. Chem. **94**, 4201–4208 (2022).

[49] G. Pileio, S. Bowen, C. Laustsen, M. C. D. Tayler, J. T. Hill-Cousins, L. J. Brown, R. C. D. Brown, J. H. Ardenkjaer-Larsen, and M. H. Levitt, "Recycling and imaging of nuclear singlet hyperpolarization," J. Am. Chem. Soc. **135**, 5084–5088 (2013).

[50] J. Eills, E. Cavallari, R. Kircher, G. Di Matteo, C. Carrera, L. Dagys, M. H. Levitt, K. L. Ivanov, S. Aime, F. Reineri, K. Münnemann, D. Budker, G. Buntkowsky, and S. Knecht, "Singlet-contrast magnetic resonance imaging: Unlocking hyperpolarization with metabolism," Angew. Chem., Int. Ed. **60**, 6791–6798 (2021).

[51] G. Pileio, J.-N. Dumez, I.-A. Pop, J. T. Hill-Cousins, and R. C. D. Brown, "Real-space imaging of macroscopic diffusion and slow flow by singlet tagging MRI," J. Magn. Reson. **252**, 130–134 (2015).

[52] C. Laustsen, G. Pileio, M. C. D. Tayler, L. J. Brown, R. C. D. Brown, M. H. Levitt, and J. H. Ardenkjaer-Larsen, "Hyperpolarized singlet NMR on a small animal imaging system," Magn. Reson. Med. **68**, 1262–1265 (2012).

[53] D. Graafen, M. B. Franzoni, L. M. Schreiber, H. W. Spiess, and K. Münnemann, "Magnetic resonance imaging of ^{1}H long lived states derived from parahydrogen induced polarization in a clinical system," J. Magn. Reson. **262**, 68–72 (2016).

[54] J.-N. Dumez, J. T. Hill-Cousins, R. C. D. Brown, and G. Pileio, "Long-lived localization in magnetic resonance imaging," J. Magn. Reson. **246**, 27–30 (2014).

[55] X. Yang, K.-R. Hu, J.-X. Xin, Y.-X. Li, G. Yang, D.-X. Wei, and Y.-F. Yao, "Multiple-targeting NMR signal selection by optimal control of nuclear spin singlet," J. Magn. Reson. **338**, 107188 (2022).

[56] A. N. Pravdivtsev, F. D. Sönnichsen, and J.-B. Hövener, "In vitro singlet state and zero-quantum encoded magnetic resonance spectroscopy: Illustration with N-acetyl-aspartate," PLOS One **15**, e0239982 (2020).

[57] S. J. DeVience, R. L. Walsworth, and M. S. Rosen, "NMR of ^{31}P nuclear spin singlet states in organic diphosphates," J. Magn. Reson. **333**, 107101 (2021).

[58] D. A. Barskiy, O. G. Salnikov, A. S. Romanov, M. A. Feldman, A. M. Coffey, K. V. Kovtunov, I. V. Koptyug, and E. Y. Chekmenev, "NMR spin-lock induced crossing (SLIC) dispersion and long-lived spin states of gaseous propane at low magnetic field (0.05 T)," J. Magn. Reson. **276**, 78–85 (2017).

[59] T. F. Sjolander, M. C. D. Tayler, A. Kentner, D. Budker, and A. Pines, "^{13}C-decoupled J-coupling spectroscopy using two-dimensional nuclear magnetic resonance at zero-field," J. Phys. Chem. Lett. **8**, 1512–1516 (2017).

[60] S. J. DeVience and M. S. Rosen, "Homonuclear J-coupling spectroscopy using J-synchronized echo detection," J. Magn. Reson. **341**, 107244 (2022).

[61] I. Schwartz, J. Scheuer, B. Tratzmiller, S. Müller, Q. Chen, I. Dhand, Z. Y. Wang, C. Müller, B. Naydenov, F. Jelezko, and M. B. Plenio, "Robust optical polarization of nuclear spin baths using Hamiltonian engineering of nitrogen-vacancy center quantum dynamics," Sci. Adv. **4**, eaat8978 (2018).

[62] B. Tratzmiller, "Pulsed control methods with applications to nuclear hyperpolarization and nanoscale NMR," Ph.D. thesis, Universität Ulm, 2021.

[63] B. Tratzmiller, J. F. Haase, Z. Wang, and M. B. Plenio, "Parallel selective nuclear-spin addressing for fast high-fidelity quantum gates," Phys. Rev. A **103**, 012607 (2021).

[64] M. Carravetta, M. Edén, X. Zhao, A. Brinkmann, and M. H. Levitt, "Symmetry principles for the design of radiofrequency pulse sequences in the nuclear magnetic resonance of rotating solids," Chem. Phys. Lett. **321**, 205–215 (2000).

[65] M. H. Levitt, "Symmetry-based pulse sequences in magic-angle spinning solid-state NMR," in *eMagRes* (John Wiley & Sons, Ltd., 2007).

[66] M. H. Levitt, "Symmetry in the design of NMR multiple-pulse sequences," J. Chem. Phys. **128**, 052205 (2008).

[67] A. Brinkmann and M. H. Levitt, "Symmetry principles in the nuclear magnetic resonance of spinning solids: Heteronuclear recoupling by generalized Hartmann–Hahn sequences," J. Chem. Phys. **115**, 357–384 (2001).

[68] D. A. Varshalovich, A. N. Moskalev, and V. K. Kheronskii, in *Quantum Theory of Angular Momentum* (World Scientific, Singapore, 1988).

[69] U. Haeberlen and J. S. Waugh, "Coherent averaging effects in magnetic resonance," Phys. Rev. **175**, 453–467 (1968).

[70] P. Mansfield, "Symmetrized pulse sequences in high-resolution. NMR in solids," J. Phys. C: Solid State Phys. **4**, 1444 (1971).

[71] U. Haeberlen, *High Resolution NMR in Solids. Selective Averaging* (Academic, New York, 1976).

[72] A. Wokaun and R. R. Ernst, "Selective excitation and detection in multilevel spin systems: Application of single transition operators," J. Chem. Phys. **67**, 1752–1758 (1977).

[73] S. Vega, "Fictitious spin 1/2 operator formalism for multiple quantum NMR," J. Chem. Phys. **68**, 5518–5527 (1978).

[74] M. H. Levitt and R. Freeman, "NMR population inversion using a composite pulse," J. Magn. Reson. **33**, 473–476 (1979).

[75] M. H. Levitt and R. Freeman, "Compensation for pulse imperfections in NMR spin echo experiments," J. Magn. Reson. **43**, 65 (1981).

[76] A. Brinkmann, M. Edén, and M. H. Levitt, "Synchronous helical pulse sequences in magic-angle spinning NMR. Double quantum recoupling of multiple-spin systems," J. Chem. Phys. **112**, 8539–8554 (2000).

[77] A. Brinkmann, J. Schmedt auf der Günne, and M. H. Levitt, "Homonuclear zero-quantum recoupling in fast magic-angle spinning nuclear magnetic resonance," J. Magn. Reson. **156**, 79–96 (2002).

[78] P. E. Kristiansen, M. Carravetta, W. C. Lai, and M. H. Levitt, "A robust pulse sequence for the determination of small homonuclear dipolar couplings in magic-angle spinning NMR," Chem. Phys. Lett. **390**, 1–7 (2004).

[79] D. H. Brouwer, P. E. Kristiansen, C. A. Fyfe, and M. H. Levitt, "Symmetry-based ^{29}Si dipolar recoupling magic angle spinning NMR spectroscopy: A new method for investigating three-dimensional structures of zeolite frameworks," J. Am. Chem. Soc. **127**, 542–543 (2005).

[80] P. E. Kristiansen, M. Carravetta, J. D. van Beek, W. C. Lai, and M. H. Levitt, "Theory and applications of supercycled symmetry-based recoupling sequences in solid-state nuclear magnetic resonance," J. Chem. Phys. **124**, 234510 (2006).

[81] M. H. Levitt, "Composite pulses," Prog. Nucl. Magn. Reson. Spectrosc. **18**, 61–122 (1986).

[82] A. J. Shaka and A. Pines, "Symmetric phase-alternating composite pulses," J. Magn. Reson. (1969) **71**, 495–503 (1987).

[83] S. Odedra, M. J. Thrippleton, and S. Wimperis, "Dual-compensated anti-symmetric composite refocusing pulses for NMR," J. Magn. Reson. **225**, 81–92 (2012).

[84] J. T. Hill-Cousins, I.-A. Pop, G. Pileio, G. Stevanato, P. Håkansson, S. S. Roy, M. H. Levitt, L. J. Brown, and R. C. D. Brown, "Synthesis of an isotopically labeled naphthalene derivative that supports a long-lived nuclear singlet state," Org. Lett. **17**, 2150–2153 (2015).

[85] M. H. Levitt, "The signs of frequencies and phases in NMR," J. Magn. Reson. **126**, 164–182 (1997).

[86] M. H. Levitt and O. G. Johannessen, "Signs of frequencies and phases in NMR: The role of radiofrequency mixing," J. Magn. Reson. **142**, 190–194 (2000).

[87] M. C. D. Tayler, "Theory and practice of singlet nuclear magnetic resonance," Ph.D. thesis, University of Southampton, 2012.

[88] M. H. Levitt, "Symmetry constraints on spin dynamics: Application to hyperpolarized NMR," J. Magn. Reson. **262**, 91–99 (2016).

[89] S. Wimperis, "Broadband, narrowband, and passband composite pulses for use in advanced NMR experiments," J. Magn. Reson., Ser. A **109**, 221–231 (1994).

[90] H. K. Cummins, G. Llewellyn, and J. A. Jones, "Tackling systematic errors in quantum logic gates with composite rotations," Phys. Rev. A **67**, 042308 (2003).

[91] J. W. Whipham, G. A. I. Moustafa, M. Sabba, W. Gong, C. Bengs, and M. H. Levitt, "Cross-correlation effects in the solution NMR spectra of near-equivalent spin-1/2 pairs," J. Chem. Phys. 104112 (2022).

[92] C. Bengs and M. H. Levitt, "SpinDynamica: Symbolic and numerical magnetic resonance in a Mathematica environment," Magn. Reson. Chem. **56**, 374–414 (2018).

[93] M. Leskes, P. K. Madhu, and S. Vega, "Floquet theory in solid-state nuclear magnetic resonance," Prog. Nucl. Magn. Reson. Spectrosc. **57**, 345–380 (2010).

[94] K. L. Ivanov, K. R. Mote, M. Ernst, A. Equbal, and P. K. Madhu, "Floquet theory in magnetic resonance: Formalism and applications," Prog. Nucl. Magn. Reson. Spectrosc. **126–127**, 17–58 (2021).